Canopy temperature and heat stress are increased by compound high air temperature and water stress, and reduced by irrigation – A modeling analysis

Xiangyu Luan[1], Giulia Vico[1]

[1]Department of Crop Production Ecology, Swedish University of Agricultural Sciences (SLU), Uppsala, Sweden

Correspondence to: Giulia Vico (giulia.vico@slu.se)

Abstract. Crop yield is reduced by heat and water stress, and even more when these conditions~~y~~ co-occur. Yet, compound effects of air temperature and water availability on crop heat stress are poorly quantified: existing crop models, by relying at least partially on empirical functions, cannot account for the feedbacks of plant traits and response to heat and water stress on canopy temperature. We developed a fully mechanistic model coupling crop energy and water balances, to determine canopy temperature as a function of plant traits, stochastic environmental conditions ~~and their variability~~; and irrigation applications. While general, the model was parameterized for wheat. Canopy temperature largely followed air temperature under well-watered conditions; but when soil water potential was more negative than -0.14 MPa, further reductions in soil water availability led to a rapid rise in canopy temperature — up to 10 °C warmer than air at soil water potential of -0.62 MPa. More intermittent precipitation led to higher canopy temperatures and longer periods of potentially damaging crop canopy temperatures. Irrigation applications aimed at keeping crops under well-watered conditions could reduce canopy temperature, but in most cases were unable to maintain it below the threshold temperature for potential heat damage; the benefits of irrigation in terms of reduction of canopy temperature ~~became smaller~~decreased as average air temperature increased. Hence, irrigation is only a partial solution to adapt to warmer and drier climates.

Keywords. Canopy temperature; heat stress; water stress; compound events; wheat; irrigation; soil water balance; canopy energy balance

1 Introduction

High and stable crop yield requires suitable climatic conditions throughout the growing season. Abiotic stressors, like water scarcity and high temperatures, can adversely affect crop growth, development, and yield, as shown by controlled-condition and field experiments, large scale surveys, and crop model applications (e.g., Zampieri et al., 2017; Daryanto et al., 2017; Kimball et al., 2016; Ray et al., 2015; Asseng et al., 2015). Both water and heat stress impair photosynthesis (Way and Yamori, 2014; Lawlor and Tezara, 2009), undermine crop growth (Hsiao, 1973; Hatfield and Prueger, 2015) and reproduction (Prasad et al., 2011), and hasten crop development and leaf senescence (Lobell et al., 2012), although the

physiological mechanisms can differ (Fahad et al., 2017). Heat and water stress do not only act independently but ~~have~~ also have compound effects on plant phenology and physiology, so that heat stress is more detrimental if co-occurring with water stress (Mahrookashani et al., 2017; Prasad et al., 2011; Suzuki et al., 2014; Cohen et al., in press). Yet, these compound effects of heat and water stress are seldom considered, experimentally and via models (Rötter et al., 2018).

Climate change is projected to increase air temperature~~s~~ and, in many regions, decrease growing season precipitation or lengthen dry spells (IPCC, 2013). Hot and dry summers are becoming more common (Zscheischler and Seneviratne, 2017; Alizadeh et al., 2020) and changes in climate are already reducing and will likely further reduce crop yield and its stability, and ultimately global food security (e.g., Challinor et al., 2014; Masson-Delmotte et al., 2018; Moore and Lobell, 2015; Rosenzweig et al., 2014). The frequency and severity of crop heat and water stress ~~is~~ are directly affected by ~~air high~~high air temperature and ~~low~~ soil water availability, and ~~is~~ are indirectly driven by ~~enhanced~~ evapotranspiration, which is enhanced ~~from~~ by warm temperatures. Nevertheless, how air temperature and precipitation, and their variability, interact in defining the occurrence, extent, and duration of crop heat and water stress has not been investigated in detail.

Canopy temperature allows more accurate estimates of the consequences of heat stress on the crop and its yield than air temperature (Gabaldón-Leal et al., 2016; Siebert et al., 2014; Rezaei et al., 2015). ~~Indeed, c~~Canopy temperature can deviate from air temperature under field conditions, because of the interplay among plant traits, plant water availability, air temperature and humidity, solar radiation, wind velocity, and the ensuing canopy microclimate (Michaletz et al., 2016; Schymanski et al., 2013). Considering canopy instead of air temperature is particularly important when characterizing the effects of compound heat and water stress, and the mitigating potential of irrigation against heat stress, because canopy temperature can be substantially higher than air temperature under water stress (e.g., Siebert et al., 2014).

Heat stress and damage are the result of complex and interacting plant physiological processes, depending on the temperature reached by the specific organ and the duration of the stress. Crop response to temperature is nonlinear (Porter and Gawith, 1999; Sanchez et al., 2014). Exceeding crop- and ~~phenological~~ developmental stage-specific thresholds can lead to plant tissue damage and halted physiological processes, although the plant can still survive. Also, the duration of exposure to high temperatures affects the outcome. For example, the accumulation of high temperature days negatively affected yield in rainfed systems (Schlenker and Roberts, 2009). In the face of increasing variability in the climatic conditions, we need to determine how stochastic precipitation and air temperature combine in determining canopy temperature. Average canopy temperatures and duration of periods above the threshold for damage can provide indications on the exposure of crops to potential heat stress.

Irrigation can buffer some aspects of climatic variability and extremes imposed on crop production (Tack et al., 2017; Zhang et al., 2015; Li and Troy, 2018; Vogel et al., 2019). Irrigation directly alleviates water stress by supplementing precipitation. Further, by sustaining the plant's evaporative cooling, irrigation can reduce canopy temperature and hence the consequences of high air temperature (Vogel et al., 2019; Siebert et al., 2017). In other words, by removing water stress, irrigation can also diminish the occurrence of heat stress. Nevertheless, we lack a quantification of how much irrigation can reduce the effects of unfavorable air temperature and precipitation, and the occurrence of crop heat stress and compound heat and water stress.

Canopy temperature is difficult to measure directly, although it can be estimated indirectly based on thermal imagery (e.g., Still et al., 2019). Models are a powerful tool to explore how canopy temperature changes with growing conditions and plant traits, beyond what is feasible via direct observations in specific experiments. Existing crop canopy temperature models either link canopy to growing conditions via simple empirical relations (e.g., Shao et al., 2019; Neukam et al., 2016) or model explicitly the leaf or canopy energy balance (Webber et al., 2016; Fang et al., 2014; Webber et al., 2017). But, so far, the role of plant water availability has been included only via semi-empirical corrections even in mechanistic models. For example, actual canopy temperature was calculated based on canopy temperatures under maximum and zero stomatal conductances and a crop water stress index (for a review of approaches and their performance, see Webber et al., 2018; Webber et al., 2017). Mechanistic models fully representing plant physiology can estimate crop canopy temperature that better reflects soil water and weather dynamics, and how plants respond to environmental conditions. Such models are currently lacking, but are necessary to quantify the effects of joint changes in air temperature and precipitation patterns; and the benefits of irrigation.

We developed a mechanistic model to estimate crop canopy temperature as a function of crop physiology, soil features, and (stochastic) climatic conditions, coupling the canopy energy balance and the water transport through the soil-plant-atmosphere continuum (SPAC), with stomatal conductance based on an optimality principle. We used the model in a case study – wheat grown in a temperate climate – to answer the following questions:

- What are the compound effects of soil water availability and air temperature on crop canopy temperature?
- How does precipitation pattern influence canopy temperature and its variability, and the duration of potentially damaging canopy temperatures?
- How effective is irrigation in reducing canopy temperature and the duration of potentially damaging canopy temperatures, depending on the climatic regime~~s~~?

2 Methods

2.1 Model description

To quantify the compound effects of air temperature and precipitation regimes on canopy temperature, and the potential of irrigation to reduce the occurrence of crop heat stress, we developed a mechanistic ~~process-based~~ model describing the coupled canopy energy and water balances, and their interactions with the water balance of the rooting zone. See the model structure in Fig. 1 and the Supplementary Information – SI – for details and symbols. The model allows exploring how plant traits and physiological responses to growing conditions interact with air temperature and soil water availability in defining canopy temperature, while relying on parameters with clear physiological meanings (Table S2).

To limit parameter and computational requirements, a minimalist approach was used, lumping the canopy in a 'big leaf' (Amthor, 1994; Jarvis and McNaughton, 1986; Bonan, 2019) and the soil water dynamics in a 'bucket-filling' model, with

instantaneous losses via runoff and percolation below the rooting zone (e.g., Milly, 1994; Rodriguez-Iturbe et al., 1999). These simplifications are expected to have minor repercussions on our conclusions (see SI, Section S5).

As detailed in the SI, combining the canopy water and energy balance, the canopy temperature, T_c, can be obtained as

$$T_c = T_a + \frac{Q^{\downarrow} + B^{\downarrow}_{n,ref} - \lambda g_{v,c} D}{c_p g_{H,c} + \lambda g_{v,c} s_s + 4\,\varepsilon_c \sigma T_a^3 \left[1 - \exp\left(-K_{bl,d}\ L_{AI}\right)\right]}. \quad (1)$$

where T_a is the air temperature; $Q^{\downarrow}$ the net absorbed short-wave radiation; $B^{\downarrow}_{n,ref}$ the net absorbed long-wave radiation at T_a (isothermal radiation); D the atmospheric vapor pressure deficit; $g_{v,c}$ and $g_{H,c}$ the total canopy conductances to water vapor and heat respectively, which include stomatal and aerodynamic conductances; λ, c_p, ε_c, σ, and $K_{bl,d}$ are constants (Table S1); s_s the slope of the vapor pressure vs. temperature curve, dependent on T_a; and L_{AI} the leaf area index.

We explicitly included the dependence of stomatal conductance on environmental conditions and plant physiology exploiting an optimality principle: plants are assumed to maximize carbon uptake over a given period, subject to limited water availability (Mäkelä et al., 1996; SI, Eq. S9-S11). We chose this approach because it is simple yet based on an evolutionary principle; and has led to promising results (Buckley et al., 2017; Eller et al., 2020). Many ~~Differently from other~~ stomatal optimization models based on water use efficiency assume that photosynthesis is limited either by RuBisCO or electron transport rate. To avoid this *a priori*~~,~~ assumption, we approximated the original Farquhar et al. (1980) model for the photosynthetic rate ~~was approximated~~ with a hyperbolic function that includes both ~~links RuBisCO and electron transport rate~~ limitations while retaining the same physiological parameters ~~of Farquhar's model~~ (Vico et al., 2013). This model was further developed here to account for the effects of the leaf boundary layer conductance and day respiration, and the key stomatal and non-stomatal effects of limited water availability on marginal water use efficiency and metabolic activity (Zhou et al., 2013; Manzoni et al., 2011; Vico and Porporato, 2008; see SI Section S1.2.1 for details). The results obtained with an alternative, empirical model of canopy conductance parameterized with eddy covariance data (SI, Eq. S30-S32; Novick et al., 2016) further support our mechanistic approach. But they ~~Those result~~ also highlighted the need to explicitly represent canopy gas exchanges to capture the dependence of canopy temperature on air temperature, unless site- and crop-specific data are available to determine the canopy conductance empirically (SI, Fig. S~~6~~9). Finally, aerodynamic conductances to heat and vapor were determined based on wind velocity, U, and leaf width, via well-established semi-empirical relations describing heat and mass transport inside the leaf boundary layer and to the bulk atmosphere (SI, Sections S1.2.2 and S1.2.3).

The canopy conductances affect and are affected by the soil water balance and water transport along the SPAC. On the one hand, soil water potential influences leaf water potential and hence leaf physiological activities (stomatal conductance, metabolic rates, and marginal water use efficiency). On the other hand, stomatal conductance and atmospheric water demand drive the rate of canopy water losses and hence the decline of soil water content. We represented the soil water content as soil saturation, s ($0 \le s \le 1$; soil moisture hereafter), linked to soil water potential, ψ_s, via texture-dependent soil water retention curves (SI, Eq. S24). A bucket-filling model was used to describe the soil moisture dynamics, with precipitation

and irrigation as input and evapotranspiration, deep percolation below the rooting zone and ~~superficial~~ surface runoff as losses, but neglecting the root structure, the time needed for the water to be redistributed within the soil, and lateral soil water movements (SI Section S1.3.1; Vico and Porporato, 2010). The soil water balance was coupled to a minimalist description of water transport through the SPAC, to determine the leaf water potential. The SPAC was modeled as a series of conductances, from the soil, through the plant, to the atmosphere (SI, Section S1.3.2; Manzoni et al., 2013).

These model components provide conductances and boundary conditions to apply Eq. (1) and quantify how canopy temperature, T_c, changes with environmental conditions and management: air temperature and humidity, wind velocity, incoming solar radiation, and precipitation; and irrigation applications, if any. The model needs to be solved iteratively (Fig. 1). At each time step (a day; see Section 2.~~2~~3), the model considers the previous soil moisture and current atmospheric conditions; ~~. T~~the previous canopy temperature and water potential are used as initial guesses for the numerical integration. First, the model determines the canopy boundary layer and aerodynamic bulk conductances and water supply and demand. Then, the canopy water potential ψ_c is determined iteratively by equating water supply and demand. After convergence is reached on ψ_c, the canopy energy balance is used to determine iteratively T_c. Finally, the soil water balance is updated with inputs and losses cumulated over the time step.

2.2 Metrics of potential heat stress damage

Based on T_c, we derived two metrics representing the potential for heat stress damage: i) $T_{c,mean}$, the mean canopy temperature during a specific period (anthesis; see Section 2.3~~2~~); and ii) P_{CHS}, the fraction of days during such period when T_c exceeded the crop-specific threshold T_{th}, above which detrimental effects of crop heat stress are likely. P_{CHS} is thus a measure of the duration of the detrimental conditions, while $T_{c,mean}$ quantifies the level of detrimental conditions.

2.~~2~~3 Case study

While the model is of general applicability, we focused on the case of wheat (*Triticum aestivum*) ~~–~~ a staple crop with relatively low tolerance to high temperatures when compared with other crops (Sanchez et al., 2014) – ~~-~~grown at 45 ° latitude N. All the model parameters are summarized in the SI, Table S2.

We restricted our analyses to anthesis, when wheat is most vulnerable to heat (Porter and Gawith, 1999) and water (Daryanto et al., 2017) stress. Anthesis was assumed to last 21 days (Mäkinen et al., 2018), starting at the 140th day of the year, i.e., May 20th (in line with observations and simulations at the latitude selected; Semenov et al., 2014; Bogard et al., 2011). For simplicity, the timing and length of anthesis ~~was~~ were kept constant under all ~~air temperature~~climatic scenarios and regardless of irrigation applications.

The model is capable of simulating the diurnal course of the key variables, but, for simplicity, we focused on the central part of the day, when incoming short-wave radiation at the top of the canopy $Q_0^{\downarrow}$ and air temperature T_a are at or near their daily

maxima, and T_c is expected to peak. Wind velocity U was assumed to be at the lowest end of its realistic range and $Q_0^{\downarrow}$ that of clear sky conditions, thus providing the maximum expected T_c and a conservative estimate of the frequency of occurrence of potentially damaging temperatures.

~~While the model can be driven by m~~Measured environmental conditions relative to a specific location could be used to force the model. Yet, ~~,~~ here ~~to systematically explore several climate scenarios, ~~we employed synthetically generated environmental conditions, varying their parameters to systematically explore several climate scenarios. ~~.~~ Daily precipitation was idealized as a marked Poisson process (Rodriguez-Iturbe et al., 1999), i.e., exponentially distributed interarrival times, with ~~the~~ average frequency λ_p. Event depth was also assumed to be exponentially distributed, with average α_p (SI, Section S1.4.2). The variability of T_a around its long-term average μ_{T_a} was described via an Ornstein-Uhlenbeck process (SI, Section S1.4.3; Benth and Benth, 2007). In line with the focus on the warmest part of the day, T_a is to be interpreted as the maximum daily air temperature. Finally, U, $Q_0^{\downarrow}$, and RH were assumed to be constant during the simulations (SI, Table S2), whereas air water vapor pressure, e_a, and vapor pressure deficit, D, were calculated based on T_a (Campbell and Norman, 1998).

As baseline pedoclimatic conditions, we considered a sandy loam soil, average precipitation frequency λ_p of 0.2 d^{-1}, average event depth α_p of 8.2 mm (corresponding to an average annual precipitation total of 600 mm), long-term average air temperature μ_{T_a} of 25 °C, air temperature standard deviation of 3.6 °C, air relative humidity RH of 40%, wind velocity U of 4 m s^{-1}, and net incoming short-wave radiation $Q_0^{\downarrow}$ of 800 W m^{-2}. We also explored additional pedoclimatic conditions. Specifically, we considered more extreme precipitation scenarios, comprising increasing precipitation ~~due to~~from increasing precipitation frequency; and a constant average annual precipitation total, but more intermittent precipitation, with reduced average precipitation frequency (λ_p=0.07 d^{-1}) and increased average event depth (α_p=23.5 mm). Long-term average air temperature μ_{T_a} also of 20 and 30 °C were explored. Separate sensitivity analyses were run for the standard deviation of air temperature (SI, Fig. S~~3~~6), soil texture (SI, Fig. S~~7~~4), and U, $Q_0^{\downarrow}$, and RH (SI, Fig. S~~5~~8).

For the irrigated case, a demand-based (water) stress-avoidance irrigation was considered, whereby an irrigation application ~~is w~~is triggered whenever soil water potential reached the intervention point, $\tilde{\psi}_s$ (Vico and Porporato, 2011). To ensure well-watered conditions, $\tilde{\psi}_s$ was set to -0.07 MPa, i.e., just above the incipient water stress for wheat (-0.1 MPa; Kalapos et al., 1996). Each irrigation application restored a pre-set target soil water potential, $\hat{\psi}_s$, set at -0.01 MPa. The difference between the intervention point and the target soil water potential is large enough to allow the use of a traditional irrigation technology (e.g., sprinkler systems or surface irrigation; see Vico and Porporato, 2011 and references therein).

Finally, the crop- and ~~phenological~~developmental-stage specific temperature threshold above which detrimental effects of crop heat stress are likely, T_{th}, was set equal to the maximum baseline temperature during anthesis. T_{th} is a large source of large uncertainty, when aiming at defining the occurrence of crop heat stress and its consequences on the crop and final yield (Siebert et al., 2017; Wanjura et al., 1992). Even within a specific developmental stage, there is a large variability of reported baseline and optimal temperatures, because of differences in variety, growing conditions, and experimental approach.

Further, crop's baseline and optimal temperatures are often defined based on air temperature, although plants respond to canopy or even organ temperature. As ~~discussed~~ showed below, the differences between air and canopy temperatures can be large, in particular under limited plant water availability. To make the comparison between T_c and T_{th} meaningful, ~~here~~ we considered a maximum baseline temperature obtained under well-watered conditions and low D; and set T_{th} equal to 30 °C (Saini and Aspinall, 1982). This value is ~~in agreement with~~similar to those obtained in other experiments focusing on wheat (Porter and Gawith, 1999).

2.~~3~~4 Statistical tests

The simulated canopy temperatures were not normally distributed, according to the Anderson-Daring test (p<0.05). Hence, to test if median $T_{c,mean}$ and P_{CHS} differed across scenarios, we employed the Mood~~'s~~ test; and to test the difference in their variances, we used the Brown-Forsythe~~'s~~ test. The test results are summarized in SI Tables S3-S8. Differences are commented on when p<0.05.

3 Results

The stochasticity of air temperature, T_a, and precipitation occurrence was mirrored by the erratic variations of soil moisture, s, and canopy temperature, T_c, in the numerically simulated trajectories (exemplified in Fig. 2). T_c largely followed T_a, but s determined whether T_c was near or above T_a. Under well-watered conditions, when s ensured unconstrained transpiration, T_c was similar to or even occasionally lower than T_a; whereas when s decreased, T_c became warmer than T_a (after approximately day 12 in Fig. 2). The evolution of T_c and other key physiological state variables, including stomatal conductance, photosynthesis and canopy water potential, during a dry down is reported in the SI, Fig. S1.

Despite the complex mechanisms linking T_a and plant water availability to T_c, the resulting temperature difference $T_c - T_a$ followed a relatively simple pattern (Fig. 3). When s was above 0.34 (corresponding to ψ_s=-0.14 MPa for the soil chosen), T_c was within 1 to 2 °C of T_a, with $T_c < T_a$ for T_a>25 °C. Conversely, for s<0.34, $T_c - T_a$ increased as s declined, with increasing slope, from 1 °C at s=0.34 to 10 °C at s=0.25 (corresponding to ψ_s=-0.62 MPa); and $T_c - T_a$ was independent of T_a (i.e., under water stress $T_c - T_a$ is driven by soil water availability for evaporative cooling). Hence, high T_c could be caused by high T_a or low s or their combination. The dependence of the plant's physiological state variable on s is reported in the SI, Fig. S2, for set T_a.

Temperature and precipitation patterns interacted in defining the mean canopy temperature during anthesis, $T_{c,mean}$. Increasing average precipitation totals decreased median $T_{c,mean}$ (colors in Fig. 4, SI Table S3, S4), in particular at lower precipitation totals (red in Fig. 4) and higher long-term ~~mean~~ average air temperature μ_{T_a} (right in Fig. 4). $T_{c,mean}$ was less affected by annual average precipitation totals larger than 900 mm and μ_{T_a} at 20 °C. $T_{c,mean}$ variability increased with μ_{T_a} and, to a lesser extent, with decreasing average precipitation totals (SI, Table S3, S4).

Precipitation regimes affected median of $T_{c,mean}$ and its variability even when considering the same precipitation total but different average precipitation frequencies, λ_p (and hence event depths, α_p; Fig. 5, top). When compared with the baseline precipitation scenario (red bars), larger but more intermittentd events (i.e., lower λ_p and higher α_p; violet bars) resulted in higher $T_{c.mean}$ median and variability in rainfed cropping (SI, Table S5). The median of $T_{c,mean}$ increased with μ_{T_a} regardless of rainfall pattern, whereas the variance ~~increased in the baseline rainfed scenario, except under more intermittent precipitation~~was not significantly affected (Table S6).

Irrigation reduced median and variance of T_c with respect to rainfed cropping under the same climatic scenario (red vs. blue hues in Fig. 5, top). Also, the dependence of T_c on precipitation pattern was reduced with irrigation (SI, Table S5). Yet, ~~even~~ despite the ~~with~~ irrigation, median and variability of T_c increased with μ_{T_a}, (SI, Table S6), although ~~such~~ the increase in median T_c was less marked than that under rainfed cropping ~~(SI, Table S6)~~.

Irrigation applications reduced the fraction of days during which T_c was above the threshold temperature for potential heat damage, T_{th}, i.e., of likely crop heat stress (P_{CHS}; Fig. 5 bottom). But it could not completely prevent this occurrence (i.e., median $P_{CHS} > 0$), except for μ_{T_a}=20 °C. Among the climatic scenarios considered, the largest ~~mean~~ median reduction in P_{CHS} (100%) occurred at μ_{T_a}= 20 °C, and the smallest (between 5~~0~~3% and 58%) ~~in the more intermittent precipitation scenario~~ at μ_{T_a}=30 °C (Table 1).

Increasing air temperature variability left median and variance of $T_{c,mean}$ unaltered in rainfed cropping, but increased them in irrigated cropping (SI, Fig. S~~3~~6 top and Table S7). There, the removal of water stress via irrigation ma~~de~~ked the resulting canopy temperature more sensitive to the air temperature regime. The median and variance of P_{CHS} increased with temperature variability~~, except the variance under the more intermittent rainfed scenario~~ in the irrigated cropping (Fig. S~~6~~3 bottom, Table S7). ~~Finer soil texture did not affect $T_{c,mean}$ and P_{CHS}, although the difference between rainfall scenarios remained (Fig. S4 and Table S8).~~ Also incoming short-wave radiation $Q_0^{\downarrow}$, wind velocity U, and air relative humidity RH affected T_c (Fig. S~~5~~8). An increase of $Q_0^{\downarrow}$ increased T_c, in particular at s<~~-~~0.35. Decreasing U enhanced T_c for s<~~-~~0.35, but did not affect it when s>0.35. In contrast, T_c slightly increased with RH for s>0.35, but showed no response to it when s< 0.35. Finer soil texture did not affect $T_{c,mean}$ and P_{CHS}, although the difference between rainfall scenarios remained (SI, Fig. S47 and Table S8). Also rooting depth $\boldsymbol{Z_r}$ could affect $T_{c,mean}$ and P_{CHS}. Yet, when considering a range of Z_r compatible with observations for wheat (and annual crops in general; Jackson et al., 1996), the effects on $T_{c,mean}$ of reduced losses via deep percolation and runoff and stabilized soil moisture with deepening roots (Laio et al., 2001) are negligible (not shown).

4 Discussion

4.1 Soil water availability and air temperature jointly affect canopy temperature

We quantified the compound effects on canopy temperature of environmental conditions: air temperature, soil water availability, incoming short-wave radiation, wind velocity, relative humidity, soil texture, and irrigation. Our model is an improvement with respect to existing approaches to simulate canopy temperature in agricultural systems, which rely on empirical corrections of values determined by means of the energy balance under extreme conditions (Fang et al., 2014; Webber et al., 2016). Lacking adequate modelling tools has limited our ability to effectively quantify the likelihood and extent of potential heat damage to crops; and the potential improvements by irrigation.

The role of environmental conditions is mediated by plant physiology and its response to conditions. Indeed losses via evapotranspiration dominated the soil water balance in all the climatic scenarios explored (see SI, Section S3.1). But, despite the complex mechanisms behind canopy temperature, the resulting pattern was relatively simple. Canopy temperature increased from cooler temperatures and wetter soils to warmer and drier conditions (Fig. 3). Under well-watered conditions, some thermoregulation occurred, cooling down or warming up the canopy depending on the air temperature, to ensure the canopy was near optimal temperature for photosynthesis (Michaletz et al., 2016).; tThis thermoregulation capability was lost when low water availability limited evaporative cooling. The differences of canopy and air temperatures obtained withprovided by the model are in line with experimental observations and other model results, thus lending support to our approach. In wheat, for example, daily maximum or mid-day canopy temperature was 2 to 10 °C higher warmer than air temperature under water stress, and from 1-to-2 °C warmer to up to 6 °C cooler than air temperature under well-watered condition, among field observations and model results (Pinter et al., 1990; Rashid et al., 1999; Jensen et al., 1990; Howell et al., 1986; Ehrler et al., 1978; Balota et al., 2008; Neukam et al., 2016; Webber et al., 2016; Schittenhelm et al., 2014; Webber et al., 2018; Mon et al., 2016). Our simulations led to canopies being 2 to 10 °C warmer than air under water stress, and to a cooling effect of 1 to 2 °C under warm but well-watered conditions. Differences between model results and observations can be ascribed to cultivar-specific traits, approach to measuring canopy temperature, measurement timing and position (within or just above the canopy), and environmental conditions (e.g., solar radiation, soil texture). Some of these aspects can be accounted for by the model, by adjusting the parameters to the specific crop and variety, and environmental conditions.

The difference between canopy and air temperature was higher than, and independent of, air temperature when soil water potential was below a critical value (Fig. 3). This threshold-like response mirrors that of stomatal closure and plant transpiration reduction with water stress (for wheat, e.g., Sadras and Milroy, 1996; Shen et al., 2002; Wang et al., 2008; Wu et al., 2011; Kalapos et al., 1996). Yet, no threshold for stomatal closure was imposed *a priori* in the model. The emerging threshold of soil water potential (-0.14 MPa) is comparable with the soil water potential corresponding to incipient stomatal closure in some experiments (-0.1 MPa; Kalapos et al., 1996), but lower higher than those of others (between -0.27 and -0.35

MPa depending on the cultivar; Wang et al., 2008) and ~~higher~~ lower than the value often assumed to correspond to well-watered conditions (-0.03 MPa; Ali et al., 1999; Laio et al., 2001).

4.2 More intermittent precipitation and higher air temperature increase canopy temperature

Climate change is expected to alter both air temperature and precipitation regimes, with further increases in average and extremely high air temperatures, and, in some regions, scarcer or more intermittent precipitation, i.e., longer dry spells (IPCC, 2013). Co-occurring dry and hot extremes are becoming increasingly frequent (Alizadeh et al., 2020; Zscheischler and Seneviratne, 2017). We showed that these compound changes can increase canopy temperature and its variability (Fig. 4 and 5).

For set air temperature conditions, even with same average precipitation totals, less frequent but larger precipitation events increased median and variance of canopy temperature, as well as the fraction of days during which the temperature threshold for potential heat damage was exceeded (Fig. 5). Larger, less frequent precipitation events result in enhanced losses via runoff and percolation below the rooting zone, thus reducing plant water availability; the ensuing (longer) dry down can thus lead to lower soil moisture levels, potentially enhancing canopy temperature. This result points to the importance of considering not only seasonal precipitation totals but also their timing. Indeed, reductions in the number of rainy days have already reduced crop yield, and could even override the benefits of increased total precipitation (Ram, 2016). For set precipitation regime,

~~A~~an increase in ~~the~~ long-term average air temperature resulted not only in a ~~-~~higher mean canopy temperature during anthesis, as expected (Eq. 1), but also in a larger variability of such mean (Fig. 4 and 5). ~~Even the extent of changes in mean canopy temperature during anthesis caused by alterations of the precipitation regimes depended on average air temperature (Fig. 5). Intermediate mean air temperature resulted in the largest response of mean canopy temperature to changes in precipitation frequency under constant average precipitation totals (Fig. 5).~~ These complex, compound effects show that it is necessary to explicitly consider not just the means but also the timing and variability of air temperature and precipitation, and their joint effects, when quantifying the potential of climate change to cause crop heat stress. Hence, models accounting in full for the stochasticity of environmental conditions are needed.

Crops are also faced by increasing air carbon dioxide (CO_2) concentration. While this further global change was not explored here, we speculate that an increase in air CO_2 concentration could reduce stomatal conductance and ~~hence~~ thus enhance canopy temperature, all the other conditions being the same. But reduced stomatal conductance can also reduce the rate of soil water storage depletion and ~~hence~~ thus the maximum canopy temperature reached during a dry down. The net result~~s~~ of an increase in air CO_2 concentration ~~is are~~is hence ~~thus~~ expected to be small. Indeed, air CO_2 concentration of 200 to 220 ppm above ambient increased canopy temperature only ~~of~~ up to 1 °C in Free Air CO_2 Enrichment experiments and in model simulations (Webber et al., 2018); and a weak reduction of yield loss to heat with enhanced CO_2 is expected (Schauberger et al., 2017).

4.3 Irrigation reduces but does not cancel the risk of heat stress

By reducing the occurrence and extent of water stress, irrigation could lower canopy temperature, and its variability, as well as the frequency of it exceeding the threshold for potential heat damage (Fig. 5). Irrigation can have positive effects on yields, not only by reducing water stress but also heat stress. Indeed, canopy-to-air temperature difference is well correlated with final yield (e.g., Blum, 1996; Reynolds et al., 1994; Thapa et al., 2018), except under extremely dry conditions (Schittenhelm et al., 2014); and often used for cultivar selection (Graß et al., 2020; Munns et al., 2010).

The extent of the reduction in canopy temperature and hence of the occurrence of potential heat stress even under stress-avoidance irrigation depended on precipitation regime and long-term average air temperature. Irrigation was particularly ~~is reduction was~~effective in reducing canopy temperature and the duration of potentially damaging conditions ~~particularly marked~~ at lower long-term average air temperature; for set long-term average air temperature, irrigation was slightly more effective ~~and~~ under more intermittent precipitation ~~(**Error! Reference source not found.**~~(Table 1). Yet, irrigation aiming at maintaining the plants under well-watered conditions could not completely remove the possibility that canopy temperature exceeded the temperature threshold for potential heat damage, except under the coolest air temperature scenario. Further, the benefits of irrigation became smaller as air temperature increased. Irrigation could also have indirect effects on canopy temperature. At the regional scale, irrigation, by enhancing evaporation, can further reduce air temperature (e.g., Sacks et al., 2009; Lobell et al., 2008a) and canopy temperature, while lengthening developmental stages. These effects could be included by altering the air temperature regime (see Fig. 3 and 4 and Table 1 for the effects of average air temperature) and the duration of the anthesis.

The risk of canopy temperature exceeding the temperature threshold for potential heat damage under (water) stress avoidance irrigation can be interpreted as the potential heat stress attributable only to air temperature. This is because no limitation to evaporative cooling is expected under the imposed irrigation scenario, where the soil water potential triggering an irrigation application was less negative ~~that~~ than the critical soil water potential emerging from Fig. 3. The reduction of the fraction of time when canopy temperature is above the threshold for potential heat damage obtained via irrigation (Table 1) is a measure of the relative ~~role~~ importance of air temperature and water stress in defining high canopy temperatures~~, thus disentangling their relative importance~~. In addition, for the most effective use of the available water resources against heat stress, the emerging threshold of soil water potential that limits water-stress induced high canopy temperatures (Fig. 3) could be used to define a crop-specific irrigation intervention point for irrigation. Maintaining the soil water potential above that threshold would require additional water resources while leading to marginal further cooling effects, i.e., little advantage in staving off heat stress.

Irrigation could not fully eliminate the negative effects of heatwaves and the warmer conditions expected in the future. But a wide-spread use of irrigation could directly or indirectly mitigate the effects of heatwaves (van der Velde et al., 2010). Nevertheless, ~~E~~even for air temperatures for which irrigation can reduce the potential for heat stress damage and considering

these regional effects, expanding irrigation to mitigate the effects of high canopy temperatures can be unadvisable or impossible, due to physical or economic water scarcity (Rosa et al., 2020), already unsustainable exploitation of water resources (Wada et al., 2010), or ~~the~~ negative impacts of irrigation on soil salt content and nearby water bodies (Daliakopoulos et al., 2016; Scanlon et al., 2007). Other management approaches are thus needed to limit the potential for crop heat stress, in particular under high average air temperatures (Deryng et al., 2011; Lobell et al., 2008b). Examples are shifting to more heat-tolerant cultivars and species (Tack et al., 2016); altering the sowing date (Lobell et al., 2014; Mourtzinis et al., 2019); or migrating crops (Sloat et al., 2020) so that anthesis occurs when air temperature is, on average, lower.

5 Conclusions

Longer dry spells and high air temperatures are expected to become even more frequent in the future, with potential negative and compound ~~ed~~ effects on crop development and yield. Exploring the occurrence and severity of crop heat stress requires quantifying canopy temperature and considering under which conditions it exceeds the temperature threshold known to create appreciable damage. We developed a mechanistic model to determine canopy temperature, based on the explicit coupling of the soil water dynamics with the canopy energy balance, and an optimality principle for stomatal functioning, mechanistically accounting for plant physiology and its response to (stochastic) environmental conditions.

Using wheat as a case study, we explored how canopy temperature and its variability changed with stochastic air temperatures and precipitation, in rainfed and irrigated cropping. When soil water potential was less negative than -0.14 MPa, the additional benefit of an increase in soil water availability and hence potential evaporative cooling became marginal; and thermoregulation ensured semi-optimal leaf temperature. However, canopy temperature rose rapidly above air temperature when soil water potential was less than -0.14 MPa, due to lowered evaporative cooling.

Less frequent and more intense precipitation caused more variable soil water contents, leading to higher and more variable canopy temperatures, and a higher fraction of days when the temperature threshold for potential heat stress damage was exceeded. Larger precipitation totals and irrigation applications could reduce the occurrence of high canopy temperature and the potential for heat damage. Yet, irrigation could not completely remove the risk of crop heat stress when long-term ~~mean~~ average air temperature was 25 °C or higher, calling for alternative management solutions.

Accurate estimates of canopy temperature are necessary to assess the role of precipitation and air temperature patterns in defining the risk of crop heat stress, and evaluate the mitigation potential of irrigation. Mechanistic models explicitly linking plant physiology to environmental conditions also allow exploring the effects of plant traits on the occurrence and extent of water and heat stress. As such, these models can support management decisions, from irrigation applications to identifying crops able to avoid heat stress.

Code availability. The MATLAB code of the model will be made available through a public repository upon acceptance of this manuscript~~The code is available upon request, by contacting the corresponding author~~.

Data availability. Data for model parameterization are available in the cited literature.

Author contributions. GV conceived the idea. XL and GV developed the codes of the model. XL performed the analyses and created the figure. XL and GV wrote the manuscript. GV revised the manuscript.

Competing interest. The authors declare that they have no competing interests.

Special issue statement. This article is submitted to the special issue "Understanding compound weather and climate events and related impacts".

Acknowledgments. We thank Maoya Bassiouni for feedback on the manuscript. The support of the Swedish Research Council (Vetenskapsrådet), under grant 2016-04910, is gratefully acknowledged. GV also acknowledges the partial support of the project COSY funded by Swedish Research Council for Sustainable Development (FORMAS, under grant 2018-02872); and the project iAqueduct, within the 2018 JPI Joint Programming Initiative Water challenges for a changing world - Water Works 2017 ERA-NET Cofound, through FORMAS grant 2018-02787.

References

Ali, M., Jensen, C., Mogensen, V., and Bahrun, A.: Drought adaptation of field grown wheat in relation to soil physical conditions, Plant Soil, 208, 149-159, https://doi.org/10.1023/A:1004535819197, 1999.

Alizadeh, M. R., Adamowski, J., Nikoo, M. R., AghaKouchak, A., Dennison, P., and Sadegh, M.: A century of observations reveals increasing likelihood of continental-scale compound dry-hot extremes, Sci Adv, 6, https://doi.org/10.1126/sciadv.aaz4571, 2020.

Amthor, J. S.: Scaling CO_2-photosynthesis relationships from the leaf to the canopy, Photos Res, 39, 321-350, https://doi.org/10.1007/bf00014590, 1994.

Asseng, S., Ewert, F., Martre, P., Rötter, R. P., Lobell, D. B., Cammarano, D., Kimball, B. A., Ottman, M. J., Wall, G. W., White, J. W., Reynolds, M. P., Alderman, P. D., Prasad, P. V. V., Aggarwal, P. K., Anothai, J., Basso, B., Biernath, C., Challinor, A. J., De Sanctis, G., Doltra, J., Fereres, E., Garcia-Vila, M., Gayler, S., Hoogenboom, G., Hunt, L. A., Izaurralde, R. C., Jabloun, M., Jones, C. D., Kersebaum, K. C., Koehler, A. K., Müller, C., Naresh Kumar, S., Nendel, C., O'Leary, G., Olesen, J. E., Palosuo, T., Priesack, E., Eyshi Rezaei, E., Ruane, A. C., Semenov, M. A., Shcherbak, I., Stöckle, C.,

Stratonovitch, P., Streck, T., Supit, I., Tao, F., Thorburn, P. J., Waha, K., Wang, E., Wallach, D., Wolf, J., Zhao, Z., and Zhu, Y.: Rising temperatures reduce global wheat production, Nat Clim Change, 5, 143-147, https://doi.org/10.1038/nclimate2470, 2015.

Balota, M., Payne, W. A., Evett, S. R., and Peters, T. R.: Morphological and physiological traits associated with canopy temperature depression in three closely related wheat lines, Crop Sci, 48, 1897-1910, https://doi.org/10.2135/cropsci2007.06.0317, 2008.

Benth, F. E., and Benth, J. Š.: The volatility of temperature and pricing of weather derivatives, Quant Finance, 7, 553-561, https://doi.org/10.1080/14697680601155334, 2007.

Blum, A.: Crop responses to drought and the interpretation of adaptation, in: Drought tolerance in higher plants: Genetical, physiological and molecular biological analysis, Springer, New York City, USA, 57-70, 1996.

Bogard, M., Jourdan, M., Allard, V., Martre, P., Perretant, M. R., Ravel, C., Heumez, E., Orford, S., Snape, J., and Griffiths, S.: Anthesis date mainly explained correlations between post-anthesis leaf senescence, grain yield, and grain protein concentration in a winter wheat population segregating for flowering time QTLs, J Exp Bot, 62, 3621-3636, https://doi.org/10.1093/jxb/err061, 2011.

Bonan, G.: Climate change and terrestrial ecosystem modeling, Cambridge University Press, Cambridge, UK, xx+438 pp., 2019.

Buckley, T. N., Sack, L., and Farquhar, G. D.: Optimal plant water economy, Plant Cell Env, 40, 881-896, https://doi.org/10.1111/pce.12823, 2017.

Campbell, G. S., and Norman, J. M.: An introduction to environmental biophysics, Springer, New York City, USA, xv+286 pp., 1998.

Challinor, A. J., Watson, J., Lobell, D. B., Howden, S. M., Smith, D. R., and Chhetri, N.: A meta-analysis of crop yield under climate change and adaptation, Nat Clim Change, 4, 287-291, https://doi.org/10.1038/Nclimate2153, 2014.

Cohen, I., Zandalinas, S. I., Huck, C., Fritschi, F. B., and Mittler, R.: Meta-analysis of drought and heat stress combination impact on crop yield and yield components, Physiol Plantarum, n/a, https://doi.org/10.1111/ppl.13203, in press.

Daliakopoulos, I., Tsanis, I., Koutroulis, A., Kourgialas, N., Varouchakis, A., Karatzas, G., and Ritsema, C.: The threat of soil salinity: A European scale review, Sci Total Environ, 573, 727-739, https://doi.org/10.1016/j.scitotenv.2016.08.177, 2016.

Daryanto, S., Wang, L., and Jacinthe, P.-A.: Global synthesis of drought effects on cereal, legume, tuber and root crops production: A review, Agr Water Manage, 179, 18-33, https://doi.org/10.1016/j.agwat.2016.04.022, 2017.

Deryng, D., Sacks, W. J., Barford, C. C., and Ramankutty, N.: Simulating the effects of climate and agricultural management practices on global crop yield, Global Biogeochem Cycles, 25, https://doi.org/10.1029/2009GB003765, 2011.

Ehrler, W., Idso, S., Jackson, R. D., and Reginato, R.: Wheat canopy temperature: Relation to plant water potential, Agron J, 70, 251-256, https://doi.org/10.2134/agronj1978.00021962007000020010x, 1978.

Eller, C. B., Rowland, L., Mencuccini, M., Rosas, T., Williams, K., Harper, A., Medlyn, B. E., Wagner, Y., Klein, T., Teodoro, G. S., Oliveira, R. S., Matos, I. S., Rosado, B. H. P., Fuchs, K., Wohlfahrt, G., Montagnani, L., Meir, P., Sitch, S., and Cox, P. M.: Stomatal optimization based on xylem hydraulics (SOX) improves land surface model simulation of vegetation responses to climate, New Phytol, 226, 1622-1637, https://doi.org/10.1111/nph.16419, 2020.

Fahad, S., Bajwa, A. A., Nazir, U., Anjum, S. A., Farooq, A., Zohaib, A., Sadia, S., Nasim, W., Adkins, S., Saud, S., Ihsan, M. Z., Alharby, H., Wu, C., Wang, D., and Huang, J.: Crop production under drought and heat stress: Plant responses and management options, Front Plant Sci, 8, 1147, https://doi.org/10.3389/fpls.2017.01147, 2017.

Fang, Q. X., Ma, L., Flerchinger, G. N., Qi, Z., Ahuja, L. R., Xing, H. T., Li, J., and Yu, Q.: Modeling evapotranspiration and energy balance in a wheat–maize cropping system using the revised RZ-SHAW model, Agr Forest Met, 194, 218-229, https://doi.org/10.1016/j.agrformet.2014.04.009, 2014.

Farquhar, G., von Caemmerer, S., and Berry, J.: A biochemical model of photosynthetic CO_2 assimilation in leaves of C3 species, Planta, 149, 78-90, https://doi.org/10.1007/BF00386231, 1980.

Gabaldón-Leal, C., Webber, H., Otegui, M., Slafer, G., Ordóñez, R., Gaiser, T., Lorite, I., Ruiz-Ramos, M., and Ewert, F.: Modelling the impact of heat stress on maize yield formation, Field Crop Res, 198, 226-237, https://doi.org/10.1016/j.fcr.2016.08.013, 2016.

Graß, R., Böttcher, U., Lilienthal, H., Wilde, P., and Kage, H.: Is canopy temperature suitable for high throughput field phenotyping of drought resistance of winter rye in temperate climate?, Eur J Agron, 120, 126104, https://doi.org/10.1016/j.eja.2020.126104, 2020.

Hatfield, J. L., and Prueger, J. H.: Temperature extremes: Effect on plant growth and development, Weather Clim Extremes, 10, 4-10, https://doi.org/10.1016/j.wace.2015.08.001, 2015.

Howell, T., Musick, J., and Tolk, J.: Canopy temperature of irrigated winter wheat, T ASAE, 29, 1692-1698, https://doi.org/10.13031/2013.30375, 1986.

Hsiao, T. C.: Plant responses to water stress, Ann Rev Plant Physio, 24, 519-570, https://doi.org/10.1146/annurev.pp.24.060173.002511, 1973.

IPCC: Climate Change 2013: The Physical Science Basis. Contribution of Working Group I to the Fifth Assessment Report of the Intergovernmental Panel on Climate Change, Cambridge University Press, Cambridge, UK, and New York, NY, USA, 1535, 2013.

Jackson, R. B., Canadell, J., Ehleringer, J. R., Mooney, H. A., Sala, O. E., and Schulze, E. D.: A global analysis of root distributions for terrestrial biomes, Oecologia, 108, 389-411, https://doi.org/10.1007/BF00333714, 1996.

Jarvis, P. G., and McNaughton, K. G.: Stomatal control of transpiration: Scaling up from leaf to region, in: Advances in Ecological Research, edited by: MacFadyen, A., and Ford, E. D., Academic Press, Cambridge, USA, 1-49, 1986.

Jensen, H., Svendsen, H., Jensen, S., and Mogensen, V.: Canopy-air temperature of crops grown under different irrigation regimes in a temperate humid climate, Irrig Sci, 11, 181-188, https://doi.org/10.1007/BF00189456, 1990.

Kalapos, T., van den Boogaard, R., and Lambers, H.: Effect of soil drying on growth, biomass allocation and leaf gas exchange of two annual grass species, Plant Soil, 185, 137-149, https://doi.org/10.1007/BF02257570, 1996.

Kimball, B. A., White, J. W., Wall, G., and Ottman, M. J.: Wheat responses to a wide range of temperatures: The hot serial cereal experiment, in: Improving Modeling Tools to Assess Climate Change Effects on Crop Response, edited by: Hatfield, J., and Fleisher, D., ASA, CSSA, SSSA, 33-44, https://doi.org/10.2134/advagricsystmodel2137.2014.0014, 2016.

Laio, F., Porporato, A., Ridolfi, L., and Rodriguez-Iturbe, I.: Plants in water-controlled ecosystems: active role in hydrologic processes and response to water stress - II. Probabilistic soil moisture dynamics, Adv Water Resour, 24, 707-723, https://doi.org/10.1016/s0309-1708(01)00005-7, 2001.

Lawlor, D. W., and Tezara, W.: Causes of decreased photosynthetic rate and metabolic capacity in water-deficient leaf cells: a critical evaluation of mechanisms and integration of processes, Ann Bot, 103, 561-579, https://doi.org/10.1093/aob/mcn244, 2009.

Li, X., and Troy, T. J.: Changes in rainfed and irrigated crop yield response to climate in the western US, Env Res Lett, 13, 064031, https://doi.org/10.1088/1748-9326/aac4b1, 2018.

Lobell, D. B., Bonfils, C. J., Kueppers, L. M., and Snyder, M. A.: Irrigation cooling effect on temperature and heat index extremes, Geophys Res Lett, 35, https://doi.org/10.1029/2008GL034145, 2008a.

Lobell, D. B., Burke, M. B., Tebaldi, C., Mastrandrea, M. D., Falcon, W. P., and Naylor, R. L.: Prioritizing Climate Change Adaptation Needs for Food Security in 2030, Science, 319, 607-610, https://doi.org/10.1126/science.1152339, 2008b.

Lobell, D. B., Sibley, A., and Ortiz-Monasterio, J. I.: Extreme heat effects on wheat senescence in India, Nat Clim Change, 2, 186-189, https://doi.org/10.1038/nclimate1356, 2012.

Lobell, D. B., Roberts, M. J., Schlenker, W., Braun, N., Little, B. B., Rejesus, R. M., and Hammer, G. L.: Greater Sensitivity to Drought Accompanies Maize Yield Increase in the U.S. Midwest, Science, 344, 516-519, https://doi.org/10.1126/science.1251423, 2014.

Mahrookashani, A., Siebert, S., Huging, H., and Ewert, F.: Independent and combined effects of high temperature and drought stress around anthesis on wheat, J Agron Crop Sci, 203, 453-463, https://doi.org/10.1111/jac.12218, 2017.

Mäkelä, A., Berninger, F., and Hari, P.: Optimal control of gas exchange during drought: Theoretical analysis, Ann Bot, 77, 461-467, https://doi.org/10.1006/anbo.1996.0056, 1996.

Manzoni, S., Vico, G., Katul, G., Fay, P. A., Polley, W., Palmroth, S., and Porporato, A.: Optimizing stomatal conductance for maximum carbon gain under water stress: a meta-analysis across plant functional types and climates, Funct Ecol, 25, 456-467, https://doi.org/10.1111/j.1365-2435.2010.01822.x, 2011.

Manzoni, S., Vico, G., Porporato, A., and Katul, G.: Biological constraints on water transport in the soil–plant–atmosphere system, Adv Water Resour, 51, 292-304, https://doi.org/10.1016/j.advwatres.2012.03.016, 2013.

Masson-Delmotte, V., Zhai, P., Pörtner, H.-O., Roberts, D., Skea, J., Shukla, P., Pirani, A., Moufouma-Okia, W., Péan, C., and Pidcock, R.: Global warming of 1.5 °C: An IPCC special report on the impacts of global warming of 1.5° C above pre-industrial levels and related global greenhouse gas emission pathways, in the context of strengthening the global response to

the threat of climate change, sustainable development, and efforts to eradicate poverty, World Meteorological Organization Geneva, Switzerland, 2018.

Michaletz, S. T., Weiser, M. D., McDowell, N. G., Zhou, J., Kaspari, M., Helliker, B. R., and Enquist, B. J.: The energetic and carbon economic origins of leaf thermoregulation, Nat Plants, 2, 16129, https://doi.org/10.1038/nplants.2016.129, 2016.

Milly, P.: Climate, soil water storage, and the average annual water balance, Water Resour Res, 30, 2143-2156, https://doi.org/10.1029/94WR00586, 1994.

Mon, J., Bronson, K. F., Hunsaker, D. J., Thorp, K. R., White, J. W., and French, A. N.: Interactive effects of nitrogen fertilization and irrigation on grain yield, canopy temperature, and nitrogen use efficiency in overhead sprinkler-irrigated durum wheat, Field Crop Res, 191, 54-65, https://doi.org/10.1016/j.fcr.2016.02.011, 2016.

Moore, F. C., and Lobell, D. B.: The fingerprint of climate trends on European crop yields, P Natl Acad Sci USA, 112, 2670-2675, https://doi.org/10.1073/pnas.1409606112, 2015.

Mourtzinis, S., Specht, J. E., and Conley, S. P.: Defining optimal soybean sowing dates across the US, Sci Rep, 9, 2800, https://doi.org/10.1038/s41598-019-38971-3, 2019.

Munns, R., James, R. A., Sirault, X. R. R., Furbank, R. T., and Jones, H. G.: New phenotyping methods for screening wheat and barley for beneficial responses to water deficit, J Exp Bot, 61, 3499-3507, https://doi.org/10.1093/jxb/erq199, 2010.

Neukam, D., Ahrends, H., Luig, A., Manderscheid, R., and Kage, H.: Integrating wheat canopy temperatures in crop system models, Agronomy, 6, https://doi.org/10.3390/agronomy6010007, 2016.

Novick, K. A., Ficklin, D. L., Stoy, P. C., Williams, C. A., Bohrer, G., Oishi, A. C., Papuga, S. A., Blanken, P. D., Noormets, A., Sulman, B. N., Scott, R. L., Wang, L., and Phillips, R. P.: The increasing importance of atmospheric demand for ecosystem water and carbon fluxes, Nat Clim Change, 6, 1023, https://doi.org/10.1038/nclimate3114, 2016.

Pinter, P. J., Zipoli, G., Reginato, R. J., Jackson, R. D., Idso, S. B., and Hohman, J. P.: Canopy temperature as an indicator of differential water use and yield performance among wheat cultivars, Agr Water Manage, 18, 35-48, https://doi.org/10.1016/0378-3774(90)90034-V, 1990.

Porter, J. R., and Gawith, M.: Temperatures and the growth and development of wheat: a review, Eur J Agron, 10, 23-36, https://doi.org/10.1016/s1161-0301(98)00047-1, 1999.

Prasad, P. V. V., Pisipati, S. R., Momcilovic, I., and Ristic, Z.: Independent and combined effects of high temperature and drought stress during grain filling on plant yield and chloroplast EF-Tu expression in spring wheat, J Agron Crop Sci, 197, 430-441, https://doi.org/10.1111/j.1439-037X.2011.00477.x, 2011.

Ram, F.: More uneven distributions overturn benefits of higher precipitation for crop yields, Env Res Lett, 11, 024004, https://doi.org/10.1088/1748-9326/11/2/024004, 2016.

Rashid, A., Stark, J. C., Tanveer, A., and Mustafa, T.: Use of canopy temperature measurements as a screening tool for drought tolerance in spring wheat, J Agron Crop Sci, 182, 231-238, 10.1046/j.1439-037x.1999.00335.x, 1999.

Ray, D. K., Gerber, J. S., MacDonald, G. K., and West, P. C.: Climate variation explains a third of global crop yield variability, Nat Comm, 6, 5989, https://doi.org/10.1038/ncomms6989, 2015.

Reynolds, M., Balota, M., Delgado, M., Amani, I., and Fischer, R.: Physiological and morphological traits associated with spring wheat yield under hot, irrigated conditions, Funct Plant Biol, 21, 717-730, https://doi.org/10.1071/PP9940717, 1994.

Rezaei, E. E., Webber, H., Gaiser, T., Naab, J., and Ewert, F.: Heat stress in cereals: mechanisms and modelling, Eur J Agron, 64, 98-113, https://doi.org/10.1016/j.eja.2014.10.003, 2015.

Rodriguez-Iturbe, I., Porporato, A., Ridolfi, L., Isham, V., and Cox, D.: Probabilistic modelling of water balance at a point: the role of climate, soil and vegetation, P Roy Soc Lond A Mat, 455, 3789-3805, https://doi.org/10.1098/rspa.1999.0477, 1999.

Rosa, L., Chiarelli, D. D., Rulli, M. C., Dell'Angelo, J., and D'Odorico, P.: Global agricultural economic water scarcity, Sci Adv, 6, eaaz6031, https://doi.org/10.1126/sciadv.aaz6031, 2020.

Rosenzweig, C., Elliott, J., Deryng, D., Ruane, A. C., Muller, C., Arneth, A., Boote, K. J., Folberth, C., Glotter, M., Khabarov, N., Neumann, K., Piontek, F., Pugh, T. A. M., Schmid, E., Stehfest, E., Yang, H., and Jones, J. W.: Assessing agricultural risks of climate change in the 21st century in a global gridded crop model intercomparison, P Natl Acad Sci USA, 111, 3268-3273, https://doi.org/10.1073/pnas.1222463110, 2014.

Rötter, R. P., Appiah, M., Fichtler, E., Kersebaum, K. C., Trnka, M., and Hoffmann, M. P.: Linking modelling and experimentation to better capture crop impacts of agroclimatic extremes-A review, Field Crop Res, 221, 142-156, https://doi.org/10.1016/j.fcr.2018.02.023, 2018.

Sacks, W. J., Cook, B. I., Buenning, N., Levis, S., and Helkowski, J. H.: Effects of global irrigation on the near-surface climate, Clim Dynam, 33, 159-175, https://doi.org/10.1007/s00382-008-0445-z, 2009.

Sadras, V. O., and Milroy, S. P.: Soil-water thresholds for the responses of leaf expansion and gas exchange: A review, Field Crop Res, 47, 253-266, https://doi.org/10.1016/0378-4290(96)00014-7, 1996.

Saini, H. S., and Aspinall, D.: Abnormal sporogenesis in wheat (*Triticum aestivum* L.) induced by short periods of high temperature, Ann Bot, 49, 835-846, https://doi.org/10.1093/oxfordjournals.aob.a086310, 1982.

Sanchez, B., Rasmussen, A., and Porter, J. R.: Temperatures and the growth and development of maize and rice: a review, Glob Change Biol, 20, 408-417, https://doi.org/10.1111/gcb.12389, 2014.

Scanlon, B. R., Jolly, I., Sophocleous, M., and Zhang, L.: Global impacts of conversions from natural to agricultural ecosystems on water resources: Quantity versus quality, Water Resour Res, 43, https://doi.org/10.1029/2006wr005486, 2007.

Schauberger, B., Archontoulis, S., Arneth, A., Balkovic, J., Ciais, P., Deryng, D., Elliott, J., Folberth, C., Khabarov, N., Muller, C., Pugh, T. A. M., Rolinski, S., Schaphoff, S., Schmid, E., Wang, X. H., Schlenker, W., and Frieler, K.: Consistent negative response of US crops to high temperatures in observations and crop models, Nat Comm, 8, 9, https://doi.org/10.1038/ncomms13931, 2017.

Schittenhelm, S., Kraft, M., and Wittich, K.-P.: Performance of winter cereals grown on field-stored soil moisture only, Eur J Agron, 52, 247-258, https://doi.org/10.1016/j.eja.2013.08.010, 2014.

Schlenker, W., and Roberts, M. J.: Nonlinear temperature effects indicate severe damages to US crop yields under climate change, P Natl Acad Sci USA, 106, 15594-15598, https://doi.org/10.1073/pnas.0906865106, 2009.

Schymanski, S. J., Or, D., and Zwieniecki, M.: Stomatal control and leaf thermal and hydraulic capacitances under rapid environmental fluctuations, Plos One, 8, e54231, https://doi.org/10.1371/journal.pone.0054231, 2013.

Semenov, M. A., Stratonovitch, P., Alghabari, F., and Gooding, M. J.: Adapting wheat in Europe for climate change, J Cereal Sci, 59, 245-256, https://doi.org/10.1016/j.jcs.2014.01.006, 2014.

Shao, Q., Bange, M., Mahan, J., Jin, H., Jamali, H., Zheng, B., and Chapman, S. C.: A new probabilistic forecasting model for canopy temperature with consideration of periodicity and parameter variation, Agr Forest Met, 265, 88-98, https://doi.org/10.1016/j.agrformet.2018.11.013, 2019.

Shen, Y., Kondoh, A., Tang, C., Zhang, Y., Chen, J., Li, W., Sakura, Y., Liu, C., Tanaka, T., and Shimada, J.: Measurement and analysis of evapotranspiration and surface conductance of a wheat canopy, Hydrol Process, 16, 2173-2187, https://doi.org/10.1002/hyp.1149, 2002.

Siebert, S., Ewert, F., Rezaei, E. E., Kage, H., and Grass, R.: Impact of heat stress on crop yield-on the importance of considering canopy temperature, Env Res Lett, 9, https://doi.org/10.1088/1748-9326/9/4/044012, 2014.

Siebert, S., Webber, H., Zhao, G., and Ewert, F.: Heat stress is overestimated in climate impact studies for irrigated agriculture, Env Res Lett, 12, https://doi.org/10.1088/1748-9326/aa702f, 2017.

Sloat, L. L., Davis, S. J., Gerber, J. S., Moore, F. C., Ray, D. K., West, P. C., and Mueller, N. D.: Climate adaptation by crop migration, Nat Comm, 11, 1243, https://doi.org/10.1038/s41467-020-15076-4, 2020.

Still, C., Powell, R., Aubrecht, D., Kim, Y., Helliker, B., Roberts, D., Richardson, A. D., and Goulden, M.: Thermal imaging in plant and ecosystem ecology: applications and challenges, Ecosphere, 10, https://doi.org/10.1002/ecs2.2768, 2019.

Suzuki, N., Rivero, R. M., Shulaev, V., Blumwald, E., and Mittler, R.: Abiotic and biotic stress combinations, New Phytol, 203, 32-43, https://doi.org/10.1111/nph.12797, 2014.

Tack, J., Barkley, A., Rife, T. W., Poland, J. A., and Nalley, L. L.: Quantifying variety-specific heat resistance and the potential for adaptation to climate change, Glob Change Biol, 22, 2904-2912, https://doi.org/10.1111/gcb.13163, 2016.

Tack, J., Barkley, A., and Hendricks, N.: Irrigation offsets wheat yield reductions from warming temperatures, Env Res Lett, 12, https://doi.org/10.1088/1748-9326/aa8d27, 2017.

Thapa, S., Jessup, K. E., Pradhan, G. P., Rudd, J. C., Liu, S., Mahan, J. R., Devkota, R. N., Baker, J. A., and Xue, Q.: Canopy temperature depression at grain filling correlates to winter wheat yield in the U.S. Southern High Plains, Field Crop Res, 217, 11-19, https://doi.org/10.1016/j.fcr.2017.12.005, 2018.

van der Velde, M., Wriedt, G., and Bouraoui, F.: Estimating irrigation use and effects on maize yield during the 2003 heatwave in France, Agriculture, Ecosystems & Environment, 135, 90-97, https://doi.org/10.1016/j.agee.2009.08.017, 2010.

Vico, G., and Porporato, A.: Modelling C3 and C4 photosynthesis under water-stressed conditions, Plant Soil, 313, 187-203, https://doi.org/10.1007/s11104-008-9691-4, 2008.

Vico, G., and Porporato, A.: Traditional and microirrigation with stochastic soil moisture, Water Resour Res, 46, https://doi.org/10.1029/2009WR008130, 2010.

Vico, G., and Porporato, A.: From rainfed agriculture to stress-avoidance irrigation: I. A generalized irrigation scheme with stochastic soil moisture, Adv Water Resour, 34, 263-271, https://doi.org/10.1016/j.advwatres.2010.11.010, 2011.

Vico, G., Manzoni, S., Palmroth, S., Weih, M., and Katul, G.: A perspective on optimal leaf stomatal conductance under CO_2 and light co-limitations, Agr Forest Met, 182, 191-199, https://doi.org/10.1016/j.agrformet.2013.07.005, 2013.

Vogel, E., Donat, M. G., Alexander, L. V., Meinshausen, M., Ray, D. K., Karoly, D., Meinshausen, N., and Frieler, K.: The effects of climate extremes on global agricultural yields, Env Res Lett, 14, 054010, https://doi.org/10.1088/1748-9326/ab154b, 2019.

Wada, Y., Van Beek, L. P., Van Kempen, C. M., Reckman, J. W., Vasak, S., and Bierkens, M. F.: Global depletion of groundwater resources, Geophys Res Lett, 37, https://doi.org/10.1029/2010GL044571, 2010.

Wang, Z.-Y., Li, F.-M., Xiong, Y.-C., and Xu, B.-C.: Soil-water threshold range of chemical signals and drought tolerance was mediated by ROS homeostasis in winter wheat during progressive soil drying, J Plant Growth Regul, 27, 309, https://doi.org/10.1007/s00344-008-9057-4, 2008.

Wanjura, D., Upchurch, D., and Mahan, J.: Automated irrigation based on threshold canopy temperature, T ASAE, 35, 153-159, https://doi.org/10.13031/2013.28748, 1992.

Way, D. A., and Yamori, W.: Thermal acclimation of photosynthesis: on the importance of adjusting our definitions and accounting for thermal acclimation of respiration, Photos Res, 119, 89-100, https://doi.org/10.1007/s11120-013-9873-7, 2014.

Webber, H., Ewert, F., Kimball, B. A., Siebert, S., White, J. W., Wall, G. W., Ottman, M. J., Trawally, D. N. A., and Gaiser, T.: Simulating canopy temperature for modelling heat stress in cereals, Environ Modell Softw, 77, 143-155, https://doi.org/10.1016/j.envsoft.2015.12.003, 2016.

Webber, H., Martre, P., Asseng, S., Kimball, B., White, J., Ottman, M., Wall, G. W., De Sanctis, G., Doltra, J., Grant, R., Kassie, B., Maiorano, A., Olesen, J. E., Ripoche, D., Rezaei, E. E., Semenov, M. A., Stratonovitch, P., and Ewert, F.: Canopy temperature for simulation of heat stress in irrigated wheat in a semi-arid environment: A multi-model comparison, Field Crop Res, 202, 21-35, https://doi.org/10.1016/j.fcr.2015.10.009, 2017.

Webber, H., White, J. W., Kimball, B. A., Ewert, F., Asseng, S., Rezaei, E. E., Pinter, P. J., Hatfield, J. L., Reynolds, M. P., Ababaei, B., Bindi, M., Doltra, J., Ferrise, R., Kage, H., Kassie, B. T., Kersebaum, K. C., Luig, A., Olesen, J. E., Semenov, M. A., Stratonovitch, P., Ratjen, A. M., LaMorte, R. L., Leavitt, S. W., Hunsaker, D. J., Wall, G. W., and Martre, P.: Physical robustness of canopy temperature models for crop heat stress simulation across environments and production conditions, Field Crop Res, 216, 75-88, https://doi.org/10.1016/j.fcr.2017.11.005, 2018.

Wu, Y., Huang, M., and Warrington, D. N.: Growth and transpiration of maize and winter wheat in response to water deficits in pots and plots, Environ Exp Bot, 71, 65-71, https://doi.org/10.1016/j.envexpbot.2010.10.015, 2011.

Zampieri, M., Ceglar, A., Dentener, F., and Toreti, A.: Wheat yield loss attributable to heat waves, drought and water excess at the global, national and subnational scales, Env Res Lett, 12, https://doi.org/10.1088/1748-9326/aa723b, 2017.

Zhang, T., Lin, X., and Sassenrath, G. F.: Current irrigation practices in the central United States reduce drought and extreme heat impacts for maize and soybean, but not for wheat, Sci Total Environ, 508, 331-342, https://doi.org/10.1016/j.scitotenv.2014.12.004, 2015.

Zhou, S., Duursma, R. A., Medlyn, B. E., Kelly, J. W., and Prentice, I. C.: How should we model plant responses to drought? An analysis of stomatal and non-stomatal responses to water stress, Agr Forest Met, 182, 204-214, https://doi.org/10.1016/j.agrformet.2013.05.009, 2013.

Zscheischler, J., and Seneviratne, S.: Dependence of drivers affects risks associated with compound events, Sci Adv, 3, https://doi.org/10.1126/sciadv.1700263, 2017.

655

Table 1: Reduction in the potential for heat stress by irrigation, as summarized by the ~~mean~~ median reductions of P_{CHS} from rainfed cropping to stress avoidance irrigation, using rainfed as reference.

μ_{T_a} (°C)	Baseline precipitation regime (α_p =8.2 mm; λ_p =0.2 d^{-1})	More intermittent precipitation (α_p =23.5 mm; λ_p =0.07 d^{-1})
20	100%	100%
25	78%	802%
30	53%	580%

660

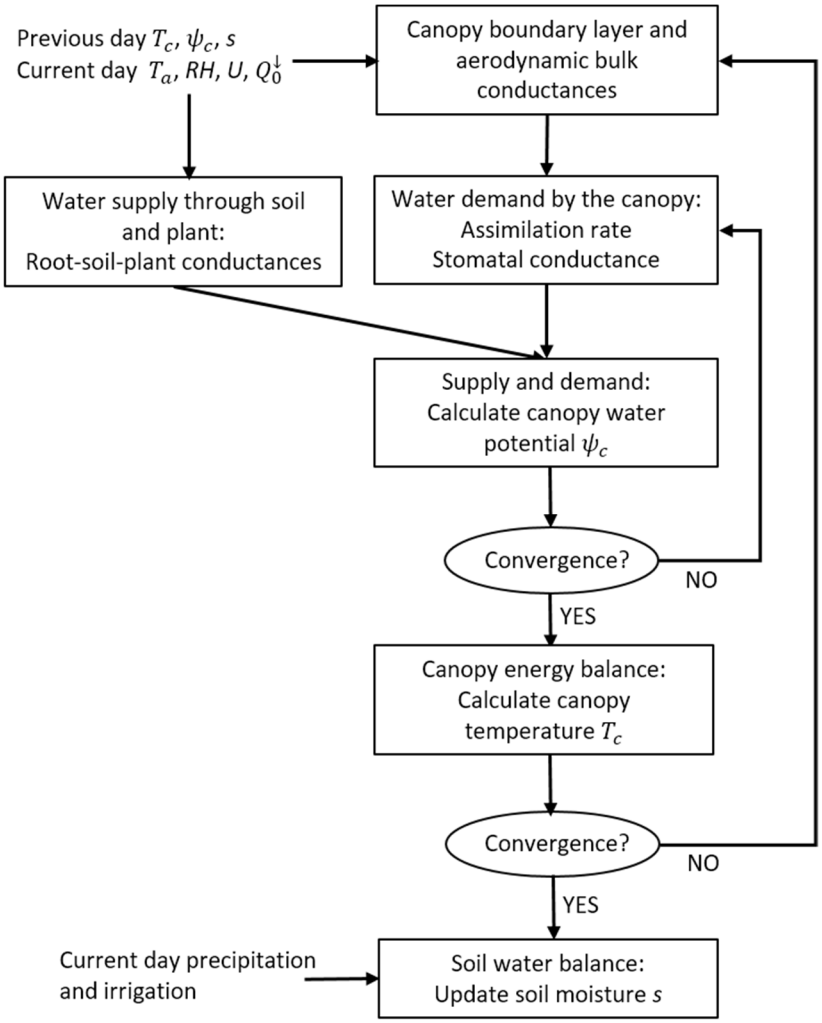

Figure 1: Flow diagram of the determination of canopy temperature and soil moisture dynamics.

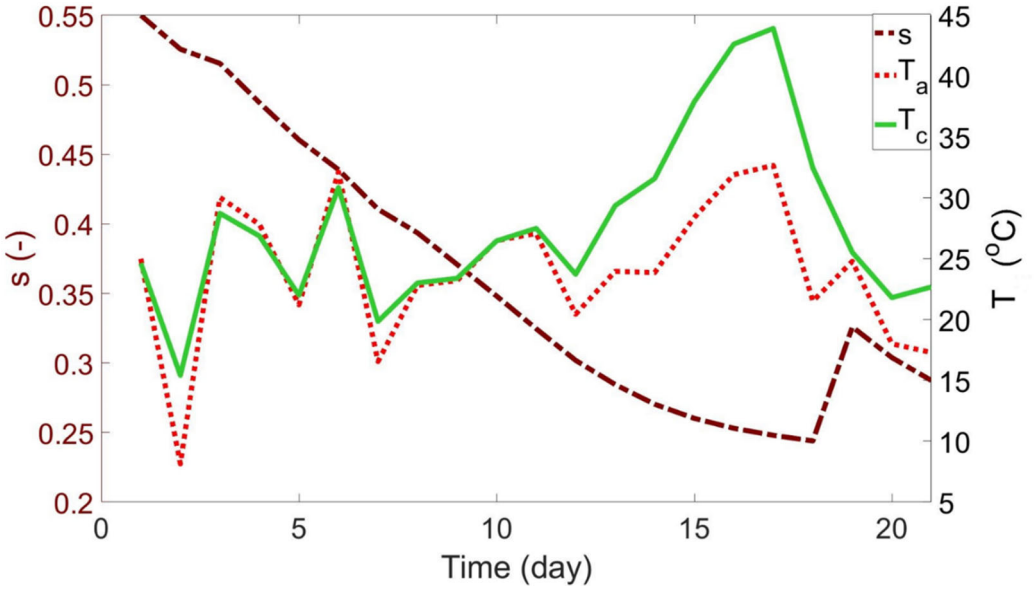

Figure 2: Example of numerically generated time series of soil moisture (s; dot-dashed burgundy line), air temperature (T_a; dotted red line), and canopy temperature (T_c; solid green line), for rainfed cropping. The left axis represents soil moisture, the right axis temperature. The model was run for 21 days with the baseline environmental conditions. Parameter values are listed in Table S2.

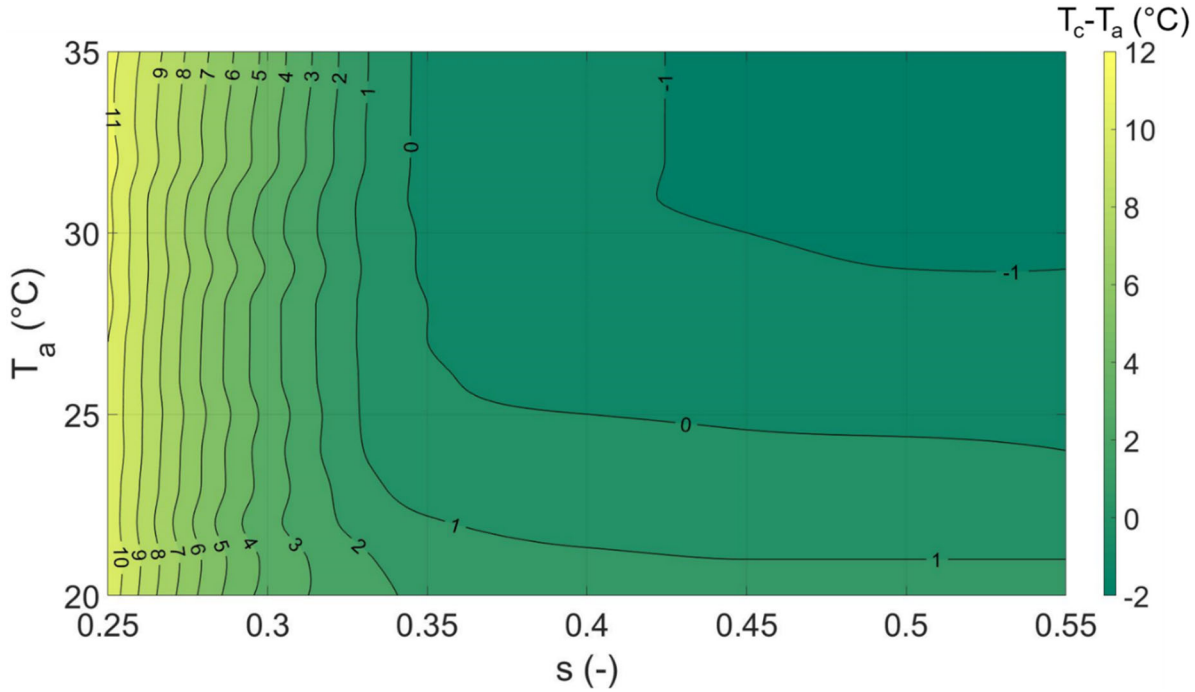

Figure 3: Canopy-air temperature difference, $T_c - T_a$ (colors and contour lines), as a function of soil moisture (s; x-axis) and air temperature (T_a; y-axis) for a sandy loam. All other parameters are summarized in Table S2.

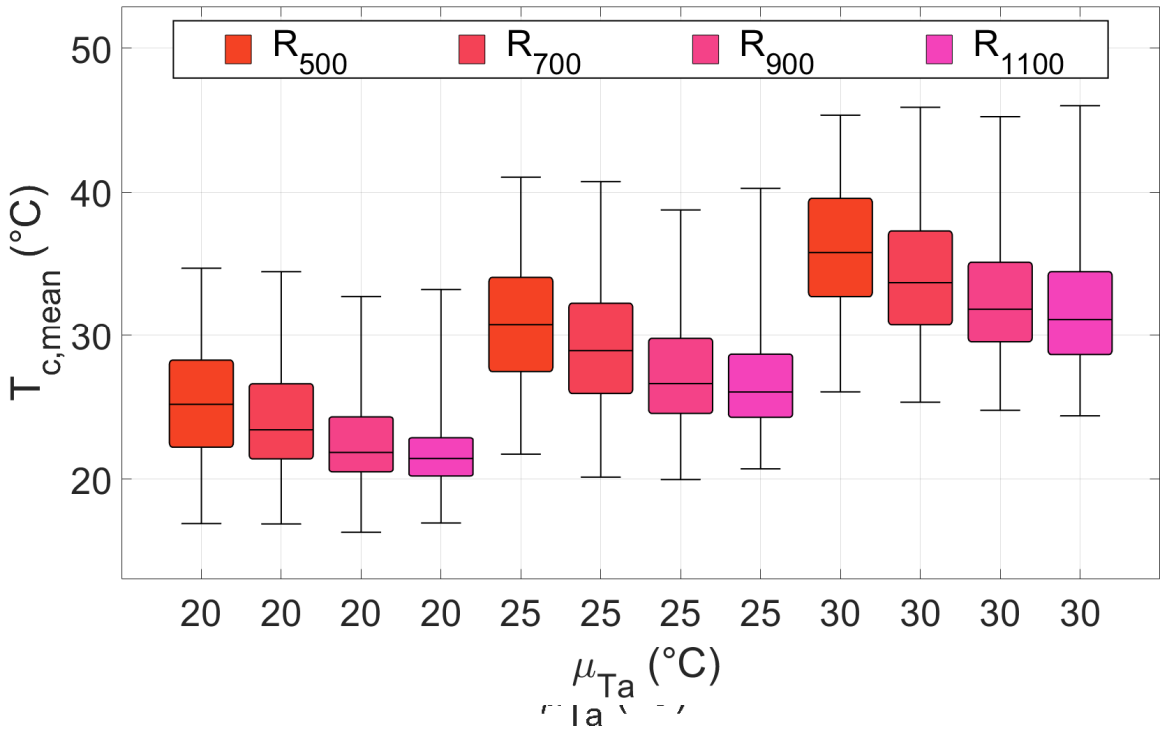

Figure 4: Distribution of mMean canopy temperatures during anthesis, $T_{c,mean}$, for four average annual precipitation totals (500, 700, 900, 1110 mm; colors) and three long-term average air temperatures μ_{T_a} (20, 25 and 30 °C; x-axis). Average precipitation depth α_p was kept at 15 mm, while average precipitation frequency λ_p changed within each group of 4 boxes, from 0.091 to 0.137, 0.183, and 0.228 d^{-1} (left to right), leading to increasing average annual precipitation totals (subscripts in the legend). For each climatic scenario, 500 21-day simulations were run. The horizontal black lines are the median values; the boxes extend from the first to the third quartile; whiskers cover the whole range.

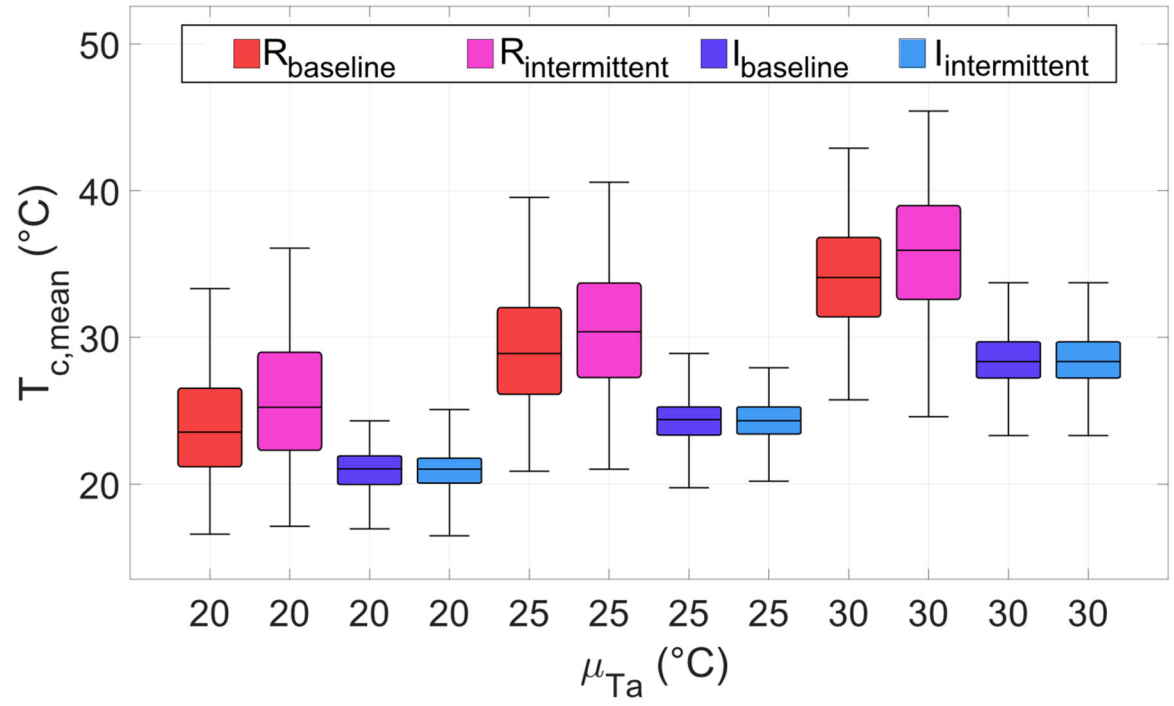
R baseline
R intermittent
I baseline
I intermittent
T c,mean (°C)
50
40
30
20
20 20 20 20 25 25 25 25 30 30 30 30
μ Ta (°C)

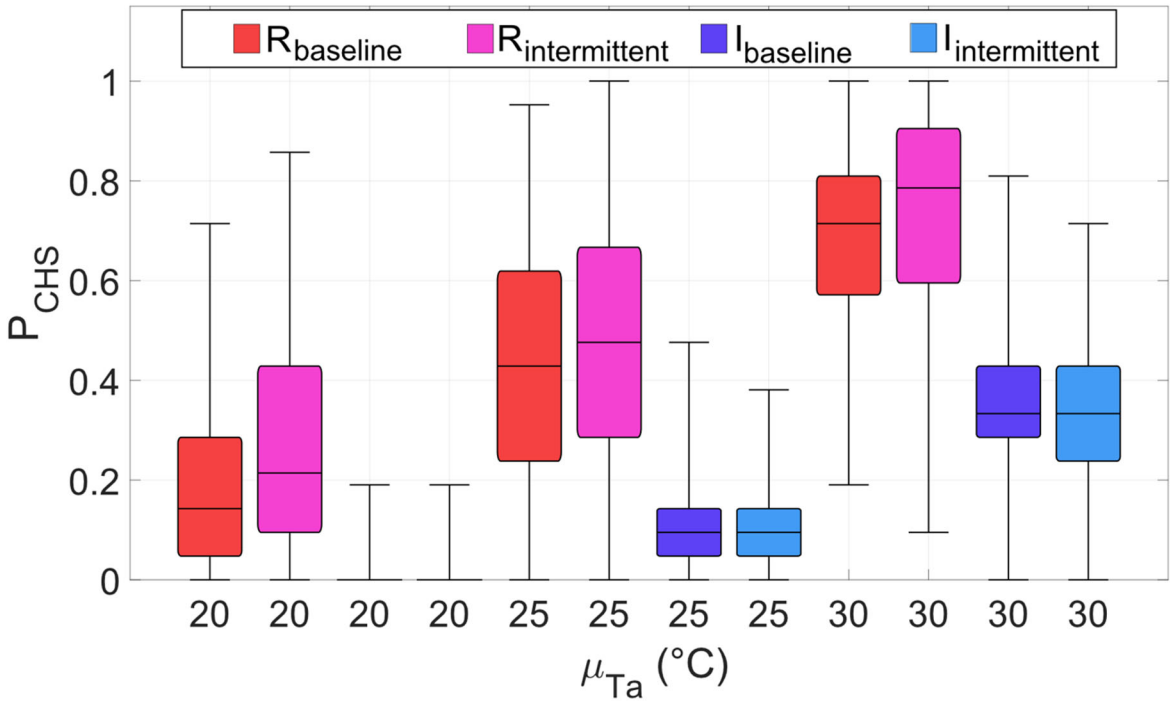
R baseline
R intermittent
I baseline
I intermittent
P CHS
1
0.8
0.6
0.4
0.2
0
20 20 20 20 25 25 25 25 30 30 30 30
μ Ta (°C)

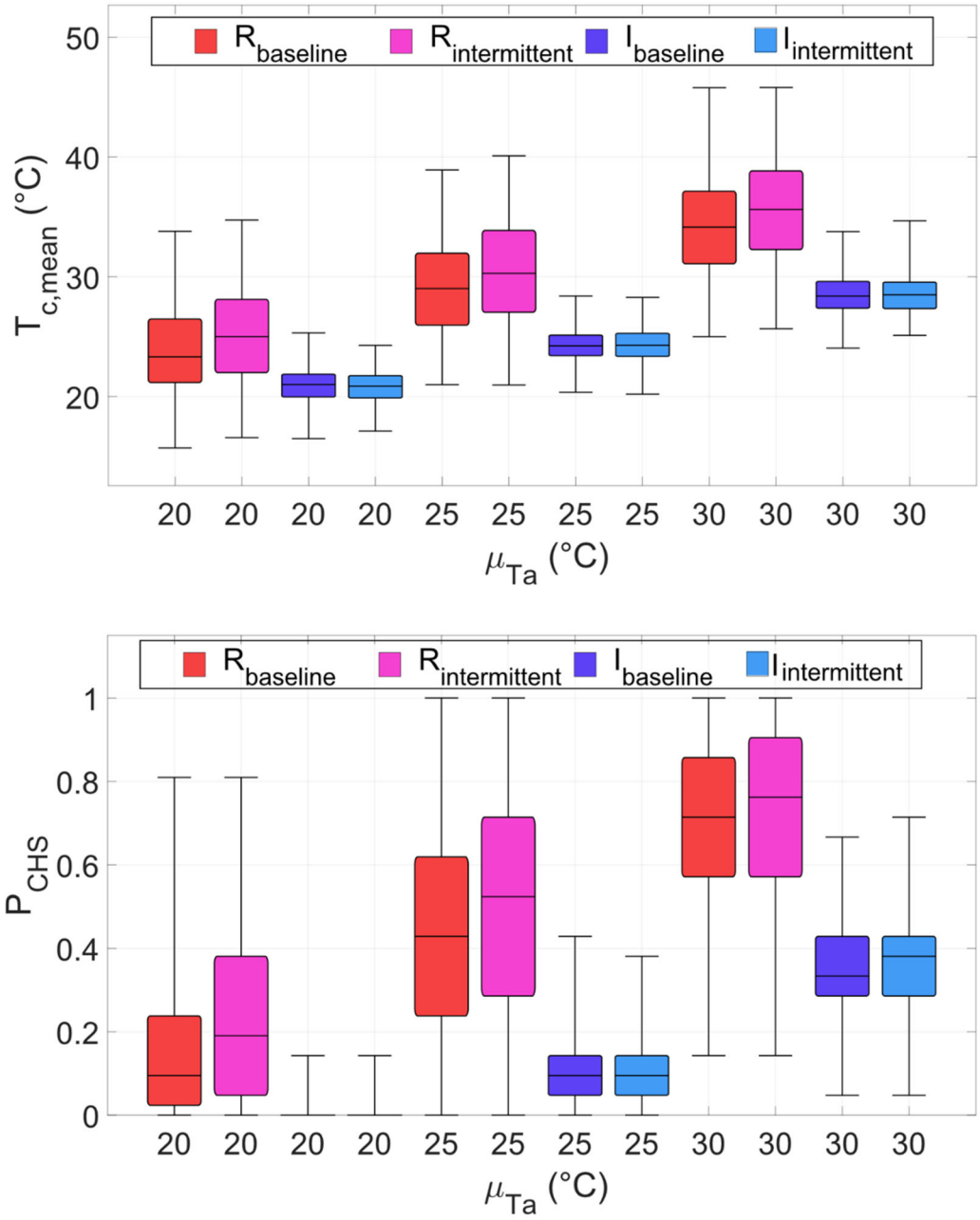

Figure 5: ~~M~~Distribution of mean canopy temperature during anthesis ($T_{c,mean}$; top) and percentage of days during which T_c is above the threshold temperature for potential heat damage, T_{th} (P_{CHS}; bottom), under three long-term average air temperatures μ_{T_a} (x-axis) and different precipitation and irrigation scenarios (colors). In each group of 4 boxes, from left to right, $R_{baseline}$ and $R_{intermittent}$ represent rainfed cropping, respectively under baseline precipitation (α_p =8.2 mm; λ_p =0.2 d^{-1}) and more intermittent precipitation (α_p =23.5 mm; λ_p =0.07 d^{-1}); $I_{baseline}$ and $I_{intermittent}$ refer to stress avoidance irrigation, under the same

precipitation regimes of the corresponding rainfed cases. For each climatic scenario, 500 21-day simulations were run. The horizontal black lines are the median values; the boxes extend from the first to the third quartile; whiskers cover the whole range.

690

Supplementary Information to

Canopy temperature and heat stress are increased by compound high air temperature and water stress, and reduced by irrigation – A modeling analysis

Xiangyu Luan[1], Giulia Vico[1]

[1]Department of Crop Production Ecology, Swedish University of Agricultural Sciences (SLU), Uppsala, Sweden

Correspondence to: Giulia Vico (giulia.vico@slu.se)

S1 Model description

To determine the canopy temperature, we developed a model considering the whole canopy as subject to the same conditions, with single exchange fluxes of energy and mass ('big-leaf model'; Tuzet et al., 2003; Bonan, 2019; Amthor, 1994; Jarvis and McNaughton, 1986), and uniform soil features and water content over the active rooting zone ('bucket filling model'; Rodriguez-Iturbe et al., 1999; Laio et al., 2001; Milly, 1994). For set conditions above the canopy (radiation, wind velocity, air temperature, and vapor pressure deficit), the model quantifies the canopy energy and water balances (Section S1.1-1.2), as a function of the canopy water potential. In turn, the canopy water potential was determined by the soil water balance and transport of water from the soil, inside the canopy to the atmosphere (Section S1.3). The whole system was forced by the conditions above the canopy and the precipitation input to the soil water balance, which were synthetically generated (Section S1.4). All the mathematical symbols are defined in Table S1. The model parameters are summarized in Table S2.

S1.1 Canopy conditions

S1.1.1 Radiation

To determine the canopy energy balance, a simplified radiation model was used, accounting for visible, near-infrared, and long-wave radiation separately (Goudriaan and Van Laar, 1994; Leuning et al., 1995). All fluxes were expressed on a per unit ground area basis.

Short-wave radiation

The incoming short-wave radiation at the top of the canopy, $Q_0^{\downarrow}$, was partitioned into the ~~near-~~near-infrared (NIR) and visible (PAR) components, $Q_{0,NIR}^{\downarrow}$ and $Q_{0,PAR}^{\downarrow}$, based on the fractions f_{NIR} and f_{PAR} respectively.

By integrating the radiation absorbed by each canopy layer within a canopy, assuming constant leaf area density (Goudriaan and Van Laar, 1994; Bonan, 2019), the total radiation absorbed by the canopy for component i (with i=NIR, PAR) was determined as (Tuzet et al., 2003):

$$Q_i^{\downarrow} = Q_{0,i}^{\downarrow}\,(1-\rho_i)\left[1-exp\left(-K_{bl}\sqrt{1-\sigma_i}\,L_{AI}\right)\right], \quad \text{(S1)}$$

where $Q_{0,i}^{\downarrow}$ is the solar radiation above the canopy in the corresponding component, ρ_i is the canopy reflection coefficient, K_{bl} is the extinction coefficient for black leaves, σ_i is the leaf scattering coefficient (so that $K_{bl}\sqrt{1-\sigma_i}$ represents the effective transmission coefficient), and L_{AI} is the canopy leaf area index.

The canopy extinction coefficient for black leaves depends on the direction of radiation and leaf orientation. Assuming an isotropic leaf angle distribution, it can be obtained as (Goudriaan and Van Laar, 1994)

$$K_{bl} = \frac{1}{2\cos\theta_{sun}}, \quad \text{(S2)}$$

where θ_{sun} is the solar zenith angle, determined based on the field location, day of the year, and time of the day (Dingman, 1994).

The canopy reflection coefficient for PAR (i=PAR) and NIR (i=NIR) was calculated as (Goudriaan and Van Laar, 1994)

$$\rho_i = 2K_{bl}\left(K_{bl}+K_{bl,d}\right)^{-1}\left(1-\sqrt{1-\sigma_i}\right)\left(1+\sqrt{1-\sigma_i}\right)^{-1}. \quad \text{(S3)}$$

where $K_{bl,d}$ is the extinction coefficient for diffuse radiation.

The total net short-wave radiation absorbed by the canopy is the ~~us~~ sum of the PAR and NIR components, $Q^{\downarrow} = Q_{PAR}^{\downarrow} + Q_{NIR}^{\downarrow}$.

Thermal (long-wave) radiation

The net absorbed long-wave radiation is the difference between the sky downward thermal radiation and the canopy upward emissivity (Leuning et al., 1995; Goudriaan and Van Laar, 1994):

$$B_n^{\downarrow} = \left(\varepsilon_a\sigma T_a^4 - \varepsilon_c\sigma T_c^4\right)\left[1-exp\left(-K_{bl,d}\;L_{AI}\right)\right] \cong B_{n,ref}^{\downarrow} + \Delta B^{\downarrow}, \quad \text{(S4)}$$

where ε_a is the apparent emissivity for a hemisphere radiating at temperature T_a (Campbell and Norman, 1998), ε_c is the canopy emissivity, σ is the Stefan-Boltzmann constant, T_a and T_c are the air and canopy temperatures respectively (expressed in Kelvin). As in Eq. (S1), the term in square brackets is the result of integrating the fluxes over the whole canopy height (Bonan, 2019), although considering the black leaf transmissivity for thermal radiation $K_{bl,d}$. The simplifying assumption was made that the long-wave radiation exchange between the bottom of the canopy and the soil surface is negligible, because, under ~~a~~ closed canopy, the soil temperature is similar to that of the canopy. The apparent emissivity depends on the cloud cover as $\varepsilon_a = \varepsilon_{a,clear}(1-0.84\,f_{cloud}) + 0.84\,f_{cloud}$, where $\varepsilon_{a,clear}$ is the clear sky emissivity, proportional to ${T_a}^2$, and f_{cloud} the cloud cover fraction (Campbell and Norman, 1998).

The expansion on the far r.h.s. of Eq. (S4) is based on the linearization of the canopy emittance term, exploiting the binomial expansion. There, $B_{n,ref}^{\downarrow}$ is the net isothermal long-wave energy absorbed by the canopy (subscript *ref*) and $\Delta B^{\downarrow}$ is the deviation from that. They were calculated as

$$\begin{matrix} B_{n,ref}^{\downarrow} = (\varepsilon_a \sigma T_a^4 - \varepsilon_c \sigma T_a^4)\left[1 - exp\left(-K_{bl,d}\, L_{AI}\right)\right] \\ \Delta B^{\downarrow} = 4\, \varepsilon_c \sigma T_a^3\, (T_a - T_c)\left[1 - exp\left(-K_{bl,d}\, L_{AI}\right)\right] \end{matrix}. \quad \text{(S5)}$$

S1.1.2 Wind velocity

To determine the wind velocity at the top of the canopy of height, h_c, $U(h_c)$, we considered the atmospheric bulk wind velocity and assumed a logarithmic wind profile above the canopy, including the diabatic corrections, i.e.,

$$U(z) = \frac{u^*}{K_v}\left[ln\left(\frac{z - d_0}{z_M}\right) + \Psi_M\right] \quad \text{(S6)}$$

Here, z is the generic height above the ground (set to h_c to determine $U(h_c)$), u^* the friction velocity, K_v the von Karman constant, d_0 the zero plane displacement ($d_0 \cong 2/3\, h_c$), z_M the roughness length for the momentum, and Ψ_M the diabatic correction factor for momentum. The diabatic correction factor was determined based on the following empirical functions, for unstable ($H \geq 0$, with H being the sensible heat flux; Eq. S20 below) and stable ($H < 0$) conditions (Campbell and Norman, 1998):

$$\Psi_M = \begin{cases} -1.2\, ln\left[\frac{1+(1-16\zeta)^{1/2}}{2}\right] & H \geq 0 \\ 6\, ln(1+\zeta) & H < 0 \end{cases}. \quad \text{(S7)}$$

ζ is the atmospheric stability, accounting for the effects of buoyancy, measured as the ratio of the convective to mechanical production of turbulence (Bonan, 2019)

$$\zeta = -\frac{K_v g (z - d_0) H}{\hat{\rho}_a c_p T_a u^{*3}}, \quad \text{(S8)}$$

where K_v is the von Karman constant, g the gravitational acceleration, z the height from the ground, $\hat{\rho}_a$ the molar density of air, c_p the heat capacity of air, T_a the air temperature at height z (expressed in Kelvin), and u^* the friction velocity. The latter was obtained by rearranging the diabatic profile equation for wind velocity at height z, $U(z)$, to yield $u^* = K_v U(z)\left[ln\left(\frac{z-d_0}{z_M}\right) + \Psi_M\right]^{-1}$.

S1.1.3 Vapor pressure deficit and air CO_2 concentration

It was assumed that turbulent transport is such that the relative humidity and the air carbon dioxide (CO_2) concentration at the canopy level are the same as the reference ones, well above the canopy.

S1.2 CO_2, water vapor, and heat canopy exchanges

S1.2.1 CO_2 assimilation and stomatal conductance

The stomatal conductance g_s was modeled based on the optimization principle, i.e., assuming that plants maximize cumulated net CO_2 uptake over a given period, subject to limited water availability. The optimization principle and the optimal control theory provide the necessary condition for the stomatal conductance g_s to be optimal as $\partial(A_{net} - \lambda_w E_l)/\partial g_s = 0$ (Mäkelä et al., 1996), where $\lambda_w = \partial A_{net} / \partial E_l$ is the marginal water use efficiency, A_{net} is the net CO_2 assimilation rate, and E_l is the transpiration rate (both expressed on a per unit leaf area basis).

In contrast to other optimization models based on water use efficiency (Katul et al., 2009; Medlyn et al., 2011), here no *a priori* assumption was made on whether photosynthesis is light- or RuBisCO- limited. Rather, the Farquhar model of photosynthesis (Farquhar et al., 1980) was approximated by a hyperbolic function, as (Vico et al., 2013)

$$A_{net} = k_1 \frac{c_i - \Gamma^*}{k_2 + c_i} - R_d, \tag{S9}$$

where c_i is the CO_2 concentration at the photosynthetic site (neglecting the mesophyll resistance), Γ^* is the CO_2 compensation point in the absence of dark respiration, R_d is the respiration rate in the light. The parameters k_1 and k_2 are related to the photosynthetic parameters as

$$k_1 = \frac{J}{4}$$
$$k_2 = \frac{J}{4}\frac{a_2}{V_{c,max}}. \tag{S10}$$

Here, J is the electron transport rate, $V_{c,max}$ the maximum carboxylation rate; and $a_2 = K_C(1 + c_{Oa}/K_O)$, with K_C and K_O being the Michelis-Menten constants for CO_2 fixation and oxygen inhibition, and c_{Oa} the oxygen concentration in the air. The electron transport rate J depends on the light-saturated electron transport rate, J_{max}, and the available photosynthetically active radiation, expressed in μmol m^{-2} s^{-1} (obtained from $Q_{PAR}^{\downarrow}$ – Eq. S1-S3, assuming a constant conversion factor of 4.6 μmol J^{-1}). The kinetic parameters (J_{max}, $V_{c,max}$, Γ^*, K_C and K_O) are a function of both canopy temperature (Bernacchi et al., 2001; Medlyn et al., 2002) and water availability (Vico and Porporato, 2008). The day respiration rate, R_d, was assumed to equal a fraction f_R of $V_{c,max}$, thus also depending on canopy temperature (and water availability).

The effects of water availability were considered directly on λ_w, $V_{c,max}$ and J_{max}. Following Zhou et al. (2013) and Manzoni et al. (2011), λ_w was assumed to be a function of the predawn canopy water potential $\psi_{c,pd}$ (set equal to the predawn soil water potential). Considering the predawn canopy water potential as opposed to the instantaneous one was motivated by λ_w not responding instantaneously to canopy water potential. A monotonically-increasing dependence on water availability was used to minimize the data needed for a robust relationship (Manzoni et al., 2011):

$$\lambda_w = \lambda_{ww}^* \frac{c_a}{c_a^*} exp(\beta_o \psi_{c,pd}), \tag{S11}$$

where λ_{ww}^{*} is the marginal water use efficiency under well-watered conditions and at reference atmospheric CO_2 concentration (c_a^{*}) and β_o is a fitting parameter describing the change in λ_w with water stress. More complex relationships have been suggested to match some observations, but they differ markedly only under extreme water stress (Manzoni et al., 2011) – conditions that are uncommon in most agricultural settings.

The effects of canopy water potential, ψ_c, on $V_{c,max}$ and J_{max} were accounted for via a Weibull-type vulnerability curve, the parameters of which were determined by fitting ~~physiological~~ leaf-level ~~observations~~ measurements (Vico and Porporato, 2008). This approach allows accounting for non-stomatal limitations to photosynthesis under water stress – a mechanism necessary to reproduce observations (Zhou et al., 2013; Drake et al., 2017).

For simplicity, canopy water potential and temperature were not included in the optimization directly, but they did affect $V_{c,max}$, J_{max} and λ_w. This is equivalent to assuming that the marginal effect of g_s on T_c and ψ_c is small with respect to that of g_s on A_{net} and E_l. It is important to emphasize that these assumptions apply only to the determination of stomatal conductance, i.e., all other modules include explicitly the roles of T_c and ψ_c.

This stomatal model represents a further development of that of Vico et al. (2013), because it explicitly includes the effects of water availability and day respiration, as well as the conductances to leaf boundary layer, and turbulent transport of vapor and heat, for more realistic estimates also under water stress and low wind velocity. The leaf boundary layer and turbulent transport in the atmosphere can act as further resistances to the vapor and CO_2 exchanges with the surrounding atmosphere and decreases with wind velocity (see Eq. S13 below). Despite the additional feedbacks included in the model, a closed formula for the optimal stomatal conductance g_s can still be obtained, but it is cumbersome and hence not reported here.

S1.2.2 Minimum leaf conductance

In parallel to the stomatal conductance, we considered a minimum conductance, g_{min}, that cannot be controlled by the plant (Kerstiens, 1996). g_{min} is known to change with water availability, although in ways that are complex, species-specific and not fully characterized yet (Duursma et al., 2019). And, while most of the experimental work has focused on the acclimation of g_{min} to low water availability as opposed to its instantaneous response, responses can occur even over few days (Bengtson et al., 1978). As a first approximation, it was assumed that g_{min} declines linearly with ψ_c, as

$$g_{min} = g_{min,ww} max\left(1 - \frac{\psi_c}{\psi_{c,0}}, 0\right) \quad \text{(S12)}$$

where $g_{min,ww}$ is the minimum conductance under well-watered conditions ($\psi_c = 0$) and $\psi_{c,0}$ is the leaf water potential at which the minimum conductance becomes negligible. Given the typically low value of $g_{min,ww}$, the exact functional dependence of g_{min} on ψ_c and its parameterization bear~~s~~ little consequences on the model outputs. Also, the role of g_{min} is negligible except under severe water stress, which, however, seldom occurs in most agricultural settings. Its inclusion ~~was motivated to~~ ensures that the model does not return unrealistic results should soil moisture reach an occasional low value during a prolonged dry down.

While g_{min} affects the amount of water lost by the leaves, it cannot be controlled by the plant and is independent of ~~the~~ stomatal conductance. So, considering in the optimization the total water losses at the leaf level, E_l, as opposed to the part stemming from the stomatal aperture only does not ~~bear any consequence in~~affect the resulting optimized stomatal conductance.

S1.2.3 Canopy boundary layer conductances

The leaf boundary layer conductances to heat and vapor per unit leaf area ($g_{H,bl}$ and $g_{v,bl}$ respectively) were quantified as (Campbell and Norman, 1998):

$$g_{H,bl} = 1.4 \cdot 0.135 \sqrt{\frac{U(h_c)}{0.7\, d_l}}, \qquad g_{v,bl} = 1.4 \cdot 0.147 \sqrt{\frac{U(h_c)}{0.7\, d_l}}, \tag{S13}$$

where d_l is the leaf width (in m; ~~and~~ the coefficient 0.7 transforms it in the leaf characteristic dimension) and $U(h_c)$ is the wind velocity at canopy height (in m s^{-1}; Eq. S6).

S1.2.4 Aerodynamic bulk conductance

A further conductance, the aerodynamic bulk conductance (per unit ground area), $g_{H,a}$, is needed to describe the turbulent transport of heat and mass from outside the leaf boundary layer to the bulk atmosphere. This conductance was determined as (Webber et al., 2016; Campbell and Norman, 1998)

$$g_{H,a} = \frac{K_v^2 \hat{\rho}_a U(z)}{\left[ln\left(\frac{z-d_0}{z_M}\right)+\Psi_M\right]\left[ln\left(\frac{z-d_0}{z_H}\right)+\Psi_H\right]}, \tag{S14}$$

where z_i is the roughness length for momentum (for i=M) and heat (for i=H), and Ψ_i is the corresponding diabatic correction factor ~~for momentum (i=M) and heat (i=H)~~. The diabatic correction factor for momentum (i=M) is given in Eq. (S7). From that, the diabatic correction factor for heat (i=H) can be determined as (Campbell and Norman, 1998)

$$\Psi_H = \begin{cases} \frac{\Psi_M}{0.6} & H \geq 0 \\ \Psi_M & H < 0 \end{cases}. \tag{S15}$$

S1.2.5 Total canopy conductances

The total canopy conductance to water vapor (per unit ground area) was calculated as the series of stomatal and cuticular conductance, leaf boundary layer conductance, and aerodynamic bulk conductance. The minimum and stomatal conductances were assumed to operate in parallel, so that the net conductance is $g_{sc} = g_{min} + g_s$ and it converges to g_{min}

during drought (as suggested by Duursma et al., 2019). This net conductance occurs in series with the leaf boundary layer conductance. Assuming that both the abaxial and adaxial side of the leaf transpire at the same rate, the total leaf-level conductance to vapor per unit leaf area is

$$g_{v,l} = \frac{g_{sc}\, g_{v,bl}}{g_{sc} + g_{v,bl}} \quad \text{(S16)}$$

The total conductance to water vapor (per unit ground area), $g_{v,c}$, is given by the series of the leaf-level conductance, and aerodynamic conductance, $g_{H,a}$,

$$g_{v,c} = \frac{L_{AI} g_{v,l}\, g_{H,a}}{L_{AI} g_{v,l} + g_{H,a}} \quad \text{(S17)}$$

where ~~the~~ L_{AI} scales up the leaf-level conductances to the canopy, exploiting the big-leaf approximation.

The total canopy conductance to heat (per unit ground area), $g_{H,c}$, is instead the series of the leaf boundary layer and aerodynamic bulk conductances, i.e.,

$$g_{H,c} = \frac{L_{AI} g_{H,bl}\, g_{H,a}}{L_{AI} g_{H,bl} + g_{H,a}} \quad \text{(S18)}$$

S1.2.6 Canopy energy balance

The canopy energy balance can be written as (Campbell and Norman, 1998)

$$Q^{\downarrow} + B_n^{\downarrow} = H + \lambda ET, \quad \text{(S19)}$$

where $Q^{\downarrow}$ and $B_n^{\downarrow}$ are the net incoming shortwave- and long-wave radiations respectively, H is the sensible heat loss, and λET is the latent heat loss, with ET being the transpiration rate (per unit ground area) and λ the latent heat of vaporization for water. The sensible heat loss depends on the temperature difference between the canopy and the air as

$$H = c_p g_{H,c} (T_c - T_a), \quad \text{(S20)}$$

The canopy transpiration rate (per unit ground area), ET, is given by

$$ET = g_{v,c} \frac{e_s(T_c) - e_a(T_a)}{P_a} \cong g_{v,c} s_s (T_c - T_a) + g_{v,c} D \quad \text{(S21)}$$

where $e_s(T_c)$ is the saturated vapor pressure at canopy temperature, $e_a(T_a)$ is the air vapor pressure, $s_s = \Delta\, {P_a}^{-1}$, with Δ being the slope of the saturation vapor pressure versus temperature function and P_a (kPa) the atmospheric pressure (Campbell and Norman, 1998), and D is the air vapor pressure deficit. The expression on the far r.h.s. was obtained exploiting Penman's linearization of the saturated vapor pressure curve and it is line with the use of Penman Monteith equation for the calculation of canopy temperature.

Substituting Eq. (S4), (S20) and (S21) in Eq. (S19), the canopy energy balance reads

$$Q^{\downarrow}_{PAR} + Q^{\downarrow}_{NIR} + B^{\downarrow}_{n,ref} + \Delta B^{\downarrow} = c_p g_{H,c}(T_c - T_a) + \lambda g_{v,c} s_s (T_c - T_a) + \lambda g_{vc} D, \quad \text{(S22)}$$

where $Q^{\downarrow}_{NIR}$ and $Q^{\downarrow}_{NIR}$ were obtained via Eq. (S1). Rearranging the terms, the canopy temperature T_c was obtained explicitly as

$$T_c = T_a + \frac{Q^{\downarrow}_{PAR} + Q^{\downarrow}_{NIR} + B^{\downarrow}_{n,ref} - \lambda g_{v,c} D}{c_p g_{H,c} + \lambda g_{v,c} s_s + 4\,\varepsilon_c \sigma T_a^3 \left[1 - exp\left(-K_{bl,d}\ L_{AI}\right)\right]}. \quad \text{(S23)}$$

S1.3 Soil water balance and water transport along the soil-plant-atmosphere continuum (SPAC)

S1.3.1 Soil water balance

To limit parameter and computational requirements, we characterized plant available water by the soil water potential, averaged over the rooting ~~depth~~zone, ψ_s, i.e., we neglected any potential inhomogeneity in root and soil water distribution in the soil volume where most of the plant roots are located. In turn, ψ_s is linked to the soil moisture, s (ranging from 0 for ~~oven~~ oven-dry soils to 1 for saturated soils) as (Clapp and Hornberger, 1978)

$$\psi_s = \psi_{s,sat}\, s^{-b}, \quad \text{(S24)}$$

where $\psi_{s,sat}$ is the soil water potential at air entry and b is an empirical exponent. Both parameters depend on soil texture.

The most effective way to determine the dynamics of the soil moisture is via the soil water balance over the active rooting zone, of depth Z_r (Rodriguez-Iturbe et al., 1999; Vico and Porporato, 2011):

$$nZ_r \frac{ds}{dt} = P + I - ET_d - LQ\,, \quad \text{(S25)}$$

where s is the soil moisture, P is the input via (effective) precipitation, I is the irrigation, if any, ET_d is the cumulated daily losses via evapotranspiration, and the term LQ combines losses via surface runoff and percolation below the rooting zone. This balance is to be interpreted at the daily time scale, so that inputs and outputs are idealized as occurring instantaneously in time. The dependence on time of the terms in Eq. (S25) is not explicitly indicated for notational clarity.

Irrigation, if any, was assumed to be demand-based, i.e., irrigation is applied when soil moisture reaches a pre-set level (the intervention point, $\tilde{s}$). Each irrigation application provides a fixed amount of water, ~~depending on the irrigation technology employed,~~ equal to $nZ_r(\hat{s} - \tilde{s})$, where $\hat{s}$ is the level of moisture restored by each irrigation application (target level) (Vico and Porporato, 2011). The soil moisture intervention point and target level were set to correspond~~s~~ to specific soil water potentials (as per Eq. S24), $\tilde{\psi}_s$ and $\hat{\psi}_s$ respectively, thus considering the ~~effect~~ role of soil texture. These parameters define the timing and amount of irrigation applications. A stress avoidance irrigation is performed when the intervention point $\tilde{\psi}_s$ is equal or less negative than the soil water potential at which incipient stomatal closure occurs; whereas, more negative $\tilde{\psi}_s$ correspond to deficit irrigation (English, 1990). The irrigation technology employed dictates the minimum water depth provided by each irrigation application, with more sophisticated approaches able to provide also smaller water depths, and

cheaper, more commonly employed technologies delivering larger water depths at each application (see, e.g., Vico and Porporato, 2011 and references therein). The target level $\hat{\psi}_s$ thus depends on both the irrigation strategy, which sets $\tilde{\psi}_s$, and the irrigation technology, which sets the depth of each application.

The losseses via evapotranspiration wereereas assumed to be dominated by losses via transpiration, in line with the focus on the anthesis phase, when canopies are closed and soil water evaporation becomes negligible (Wei et al., 2017). The cumulated daily losses via evapotranspiration was were thus determined by cumulating the losses via canopy transpiration, ET (Eq. S21), during the day. The model was run only once per day, under the conditions likely resulting in the highest canopy temperatures (see Section 2.23 in the main text). To scale up the estimated losses via evapotranspiration at the daily scale, the dailywe assumed evapotranspiration rate was assumed to followed a parabolic diurnal evolution. Hence, the total daily losses via evapotranspiration wereas determined as

$$ET_d = \frac{2}{3} ET\ (t_{sunset} - t_{sunrise}), \tag{S26}$$

where $t_{sunset} - t_{sunrise}$ is the day length, i.e., the time between sunrise and sunset.

Finally, in line with the daily interpretation of the water balance in Eq. (S25), losses via surface runoff and deep percolation below to the rooting zone, LQ, were assumed to occur instantaneously when soil moisture exceeds a threshold s_1, slightly above the soil field capacity. Hence, soil moisture dynamics is effectively upper-bounded by s_1.

S1.3.2 Soil-plant-atmosphere continuum

The soil water balance was coupled to a minimalist description of the soil-plant-atmosphere continuum (SPAC), to determine the leaf water potential. Water moves along the SPAC as driven by gradients of total water potential, from the soil to the leaf, and then to the atmosphere. Based on the electric analogy, the water flow was modulated by a series of resistances (or conductances): soil to root conductance; root to leaf (i.e., xylem) conductance; and leaf to the atmosphere (i.e., stomatal conductance). These conductances depend on soil features and plant traits, and decline with decreasing water potential. Details on these dependencies and parameter values are summarized in Manzoni et al. (2013).

S1.4 Environmental conditions above the canopy

The model requires solar radiation, air temperature, and humidity in the bulk atmosphere, at height $z > h_c$, as well as the daily precipitation totals. To systematically explore different climatic scenarios, these environmental conditions were synthetically generated, as described next.

S1.4.1 Solar radiation

The total incoming short-wave solar radiation, $Q_0^{\downarrow}$, was set to a realistic and constant value. Clear sky conditions were assumed for the entire anthesis period, thus likely leading to an overestimate of T_c and a conservative estimate of the potential for heat damage.

S1.4.2 Precipitation

Daily precipitation was idealized as a marked Poisson process, i.e., with exponentially distributed interarrival times, τ_p (Rodriguez-Iturbe et al., 1999):

$$p_{\tau_p}(\tau_p) = \lambda_p \, e^{-\lambda_p \tau_p}, \quad \tau_p \geq 0, \tag{S27}$$

where λ_p is the average frequency of precipitation occurrence.

Each precipitation was assumed to occur instantaneously at the daily time scale (i.e., the temporal structure of precipitation is ignored). Each event provides a random ~~amount~~ amount h_p, assumed to be exponentially distributed

$$p_{h_p}(h_p) = \frac{1}{\alpha_p} \, e^{-\frac{1}{\alpha_p} h_p}, \quad h_p \geq 0, \tag{S28}$$

with α_p corresponding to the average precipitation depth.

With this model of precipitation, the average total annual precipitation is $365\alpha_p\lambda_p$.

S1.4.3 Air temperature

Since the focus was on the warmest part of the day, we interpreted T_a as the daily maximum temperature. The day-to-day fluctuations of T_a were described as an Ornstein-Uhlenbeck process (Benth and Benth, 2007). The rate of air temperature change was thus expressed as

$$\frac{dT_a}{dt} = -\frac{1}{\tau_{T_a}}\left(T_a - \mu_{T_a}\right) + \sqrt{k_3}\eta_t \tag{S29}$$

where τ_{T_a} is the relaxation time (i.e., ${\tau_{T_a}}^{-1}$ is the mean-~~-~~reversion rate of the process); μ_{T_a} is the long-term ~~mean of~~average maximum daily temperature~~s~~; k_3 is the diffusion parameter, quantifying the noise 'size'; and η_t is a Gaussian white noise (with vanishing mean, unit variance and an autocorrelation with a sharp peak in zero and dropping to zero for any lag greater than 0; Ridolfi et al., 2011). With these assumptions, T_a has a Gaussian distribution, with mean μ_{T_a} and standard deviation $\left(\tau_{T_a} k_3 / 2\right)^{1/2}$.

S1.4.4 Wind velocity and relative humidity

Wind velocity and relative humidity above the canopy were assumed to be constant during the simulations.

S1.5 Numerical simulations

For each climate and irrigation scenario, and soil type, we ~~run ran~~ran 501 simulations, each lasting 21 days (the duration of the heading period under current climatic conditions; Mäkinen et al., 2018). The initial conditions for soil water content and air temperature for each 21-day simulation ~~correspond~~ were set equal to the final conditions for the previous 21-day simulation, i.e., the simulations were concatenated~~.~~. In such a way, the conditions at the beginning of each period are fully stochastic and reflect a long period of operation of all the hydrological processes, including the ~~reflect the effects of~~ previously~~-~~-occurred conditions – an aspect particularly important for the soil water balance. For the first simulation, the initial soil water potential was set at $\hat{\psi}_s$ and initial air temperature at μ_{T_a}, but this simulation was excluded from the analyses to limit the influence of these arbitrary choices.

The model was solved via nested numerical iterations (Fig. 1 in the main text). For each day, air temperature and precipitation inputs were generated as detailed in Section S1.4. The T_c at the previous time step was used to determine the diabatic corrections and hence the aerodynamic conductance and the wind velocity, while ψ_c at the previous time step was used to estimate the aerodynamic and boundary layer conductances, the soil-to-leaf, and optimal stomatal conductances (Eq. S6-S8, S12-S18). Then, the resulting water demand (driven by g_s, T_c, ~~and~~ ψ_s, and D) was compared with the water supply through the soil, root, and plant (driven by the series of soil to root to plant conductances, and the difference in water potential between the soil and the canopy). The ψ_c for which supply ~~equaled~~equalled demand was calculated and used in the subsequent iteration, ~~where~~ when the values of conductances were updated. Once convergence on ψ_c was reached (i.e., when the absolute difference in ψ_c between two subsequent steps was smaller than $\psi_{c,toler}$), the iterative loop on ψ_c was exited, and the g_s value corresponding to such ψ_c was used in the canopy energy balance, to obtain a new estimate of T_c. This whole ~~-~~cycle was repeated till convergence was reached also on T_c (with tolerance $T_{c,toler}$), unless a pre-set ~~maximum~~ number of iterations Max_{iter} was reached.

Once T_c was determined, the mid-day losses via transpiration were calculated and scaled up to the daily level (Eq. S26), and the daily soil moisture balance was updated, including any input via precipitation or irrigation. The new soil moisture s was used as the basis to determine the soil water potential for the subsequent day.

Table 1: List of symbols.

Variable	Description	Units
a_2	Combination of the Michelis Menten constants for CO_2 fixation and oxygen inhibition	µmol mol^{-1}
A_{net}	Net CO_2 assimilation rate (per unit leaf area)	µmol m^{-2} s^{-1}
b	Exponent of soil water retention curve	-
$B_n^{\downarrow}$	Net incoming long-wave radiation	W m^{-2}
$B_{n,ref}^{\downarrow}$	Net isothermal long-wave energy absorbed by the canopy	W m^{-2}
c_a^*	Reference CO_2 concentration in the bulk atmosphere	µmol mol^{-1}
c_i	CO_2 concentration at the photosynthetic site	µmol mol^{-1}
c_{Oa}	Oxygen concentration in the bulk atmosphere	mmol mol^{-1}
c_p	Heat capacity of air	J kg^{-1} K^{-1}
d_0	Zero plane displacement	m
d_l	Leaf width	m
D	Vapor pressure deficit	mol mol^{-1}
$e_a(T_a)$	Air vapor pressure at air temperature T_a	mol m^{-2} s^{-1}
$e_s(T_c)$	Saturation vapor pressure at canopy temperature T_c	mol m^{-2} s^{-1}
ET	Instantaneous evapotranspiration rate (per unit ground area)	mol m^{-2} s^{-1}
ET_d	Daily evapotranspiration rate (per unit ground area)	m s^{-1}
ET_l	Instantaneous evapotranspiration rate (per unit leaf area)	mol m^{-2} s^{-1}
f_{cloud}	Cloud cover fraction	-
f_{NIR}	Fraction of total radiation in the NIR wavebands	-
f_{PAR}	Fraction of total radiation in the PAR wavebands	-
f_R	Ratio between R_d and $V_{c,max}$	-
g	Gravitational acceleration	m s^{-2}
$g_{H,a}$	Aerodynamic bulk conductance (per unit ground area)	mol m^{-2} s^{-1}
$g_{H,bl}$	Leaf boundary layer conductance to heat (per unit leaf area)	mol m^{-2} s^{-1}
$g_{H,c}$	Total canopy conductance to heat (per unit ground area)	mol m^{-2} s^{-1}
g_{min}	Minimum conductance (i.e., conductance that cannot be controlled by the	mol m^{-2} s^{-1}

	plant; per unit leaf area)	
$g_{min,ww}$	Minimum conductance under well-water condition (per unit leaf area)	mol m^{-2} s^{-1}
g_s	Stomatal conductance (per unit leaf area)	mol m^{-2} s^{-1}
g_{sc}	Sum of stomatal and minimum conductance (per unit leaf area)	mol m^{-2} s^{-1}
$g_{v,c}$	Total canopy conductance to water vapor (per unit ground area)	mol m^{-2} s^{-1}
$g_{v,bl}$	Leaf boundary layer conductance to water vapor (per unit leaf area)	mol m^{-2} s^{-1}
$g_{v,l}$	Leaf-level conductance to water vapor (per unit leaf area)	mol m^{-2} s^{-1}
$G_{S,ref}$	Reference ~~surface~~ canopy conductance (per unit ground area)~~rate~~	mmol · m^{-2} · s^{-1}
G_s	~~Surface~~ Canopy conductance (per unit ground area)	mmol · m^{-2} · s^{-1}
h_c	Canopy height	m
h_p	Precipitation event depth	m
H	Sensible heat flux	W m^{-2}
I	Irrigation application	m d^{-1}
J	Electron transport rate	µmol m^{-2} s^{-1}
J_{max} ($J_{max,25}$)	Maximum electron transport rate (and reference value at 25 °C)	µmol m^{-2} s^{-1}
k_1	Parameter of the hyperbolic photosynthetic model (Eq. (S10))	µmol m^{-2} s^{-1}
k_2	Parameter of the hyperbolic photosynthetic model (Eq. (S10))	µmol mol^{-1}
k_3	Diffusion parameter of air temperature (noise 'size')	$°C^2$ d^{-1}
K_{bl}	Extinction coefficient for black leaves	-
$K_{bl,d}$	Extinction coefficient for black leaves, under diffuse light and long-wave radiation	-
K_C	Michelis-Menten constants for CO_2 fixation	µmol mol^{-1}
K_O	Michelis-Menten constants for oxygen inhibition	mmol mol^{-1}
K_{sat}	Soil hydraulic conductivity at saturation	m d^{-1}
K_v	Von Karman constant	-
L_{AI}	Leaf area index	m^2 m^{-2}
LQ	Surface runoff and deep percolation below the rooting ~~depth~~zone	m d^{-1}
m	Slope of surface conductance to water pressure deficit	$[ln(kPa)]^{-1}$
Max_{iter}	Maximum iteration number	-

n	Soil porosity	-
P	Daily total precipitation	m d^{-1}
P_a	Air pressure	kPa
P_{CHS}	Fraction of days during which T_c exceeded T_{th}	-
$Q^{\downarrow}$	Total net short-wave radiation absorbed by the canopy	W m^{-2}
$Q_{0,i}^{\downarrow}$	Solar radiation above the canopy (i= NIR, PAR)	W m^{-2}
$Q_i^{\downarrow}$	Total radiation of the component (i= NIR, PAR)	W m^{-2}
R_d	Respiration rate in the light	μmol m^{-2} s^{-1}
RH	~~Air relative~~Relative air humidity	-
s	Soil moisture	-
s_s	Slope of the vapor pressure vs. temperature curve	kPa K^{-1}
s_1	Soil moisture above which runoff and percolation below the active rooting zone occur instantaneously	-
t	Time	d
$t_{sunrise}$, t_{sunset}	Time of sunrise, time of sunset	hr
T_a	Air temperature	°C
T_c	Canopy temperature	°C
$T_{c,toler}$	Canopy temperature tolerance for the numerical simulations	°C
T_{th}	Threshold above which crop heat stress occurs ~~around~~ during the anthesis period	°C
u^*	Friction velocity	m s^{-1}
$U(z)$	Mean wind velocity at height z	m s^{-1}
$V_{c,max}$ ($V_{c,max,25}$)	Maximum carboxylation rate (and reference value at 25 °C)	μmol · m^{-2} · s^{-1}
z	Height from the ground	m
z_M	Roughness length for the momentum	m
z_U	Height of wind measurement	m
Z_r	Active rooting depth	m
α_p	Average precipitation event depth	m
β_o	Fitting parameter of the marginal water use efficient response function to	-

	water stress	
Γ^*	CO_2 compensation point in the absence of dark respiration	mol mol^{-1}
Δ	Slope of the vapor pressure vs. temperature curve	mol mol^{-1} K^{-1}
$\Delta B^{\downarrow}$	Deviation of absorbed energy	W m^{-2}
ε_a	Apparent long-wave emissivity for a hemisphere radiating at temperature T_a	-
$\varepsilon_{a,clear}$	Clear sky emissivity	-
ε_c	Long-wave canopy emissivity	-
ζ	Atmospheric stability	-
θ_{sun}	Solar zenith angle	rad
λ	Latent heat of vaporization for water	J kg^{-1}
λ_p	Average precipitation frequency	day^{-1}
λ_w	Marginal water use efficiency	mol mol^{-1}
λ_{ww}^*	Marginal water use efficiency under well-watered condition and reference air CO_2 concentration	mol mol^{-1}
μ_{T_a}	Long-term ~~mean~~ average air temperature	°C
$\hat{\rho}_a$	Molar density of air	mol m^{-3}
ρ_i	Canopy reflection coefficient for PAR (*i*=PAR) and NIR (*i*=NIR)	-
σ	Stefan-Boltzman constant	W m^{-2} K^{-4}
σ_i	Leaf scattering coefficient for PAR (*i*=PAR) and NIR (*i*=NIR)	-
τ_p	Precipitation interarrival time	d
τ_{T_a}	Relaxation time (i.e., ${\tau_{T_a}}^{-1}$ is the mean-reversion rate of the Ornstein-Uhlenbeck process)	d
$\psi_{c,0}$	Leaf water potential at which minimum conductance becomes negligible	MPa
ψ_c	Canopy water potential	MPa
$\psi_{c,pd}$	Predawn canopy water potential	MPa
$\psi_{c,toler}$	Canopy water potential tolerance for the numerical simulations	MPa
ψ_s	Soil water potential	MPa
$\tilde{\psi}_s$	Irrigation intervention soil water potential	MPa

$\hat{\psi}_s$	Target soil water potential for irrigation	MPa
$\psi_{s,sat}$	Soil water potential at saturation	MPa~~A~~
Ψ_i	Diabatic correction factor (*i*= H for heat; *i*=M for momentum)	MPa

Table S2: List of parameters.

Symbol	Value	Unit	Source
Crop parameters			
C_d	0.3	-	(Katul et al., 2004; crop canopies)
d_0	2/3 h_c	m	(Jones, 1992)
d_l	0.04	m	
f_R	0.01	-	
$g_{min,ww}$	1.73×10^{-2}	mmol · m^{-2} · s^{-1}	(Duursma et al., 2019; mean value for wheat)
h_c	0.6	m	
$J_{max,25}$	132	µmol · m^{-2} · s^{-1}	(Wullschleger, 1993; wheat)
K_c	405	µmol mol^{-1}	
K_O	278	mmol mol^{-1}	
L_{AI}	2	m_{leaf}^2 m_{ground}^{-2}	~~(Vico and Porporato, 2008)~~
T_{th}	30	°C	(Saini and Aspinall, 1982)
$V_{c,max,25}$	83	µmol · m^{-2} · s^{-1}	(Wullschleger, 1993; wheat)
Z_r	0.3	m	(Jackson et al., 1996)
β_o	-1.26	MPa^{-1}	(Manzoni et al., 2011; median value for forbs and grasses in mesic and wet climates)
λ_{ww}^*	981	mol mol^{-1}	(Manzoni et al., 2011; median value for forbs and grasses in mesic and wet climates)
$\psi_{c,0}$	-3	MPa	
Environmental conditions			

c_a^*	400	µmol mol^{-1}	
C_{Oa}	210	mmol mol^{-1}	
k_3	32.6	°C^2 d^{-1}	(Rigby and Porporato, 2008)
RH	40%	-	
P_a	101	kPa	
$Q_0^{\downarrow}$	800	W m^{-2}	
$U(z_U)$	4	m s^{-1}	
z_M	0.13 h_c	m	(Jones, 1992)
z_U	2	m	
α_p	8.2 (baseline scenario)	mm	~~Baseline scenario~~
λ_p	0.2 (baseline scenario)	d^{-1}	~~Baseline scenario~~
μ_{T_a}	25 (baseline scenario)	°C	~~Baseline scenario~~
τ_{T_a}	0.81	d	(Rigby and Porporato, 2008)
Soil parameters			
b	4.38 (loamy sand) 4.90 (sandy loam) 5.39 (loam)	-	(Laio et al., 2001)
n	0.42 (loamy sand) 0.43 (sandy loam) 0.45 (loam)	-	(Laio et al., 2001)
K_{sat}	1.0 (loamy sand) 0.8 (sandy loam) 0.2 (loam)	m d^{-1}	(Laio et al., 2001)
s_1	0.57 (sandy loam), 0.62 (loamy sand) 0.72 (loam)	-	(Laio et al., 2001)
$\tilde{\psi}_s$	-0.07	MPa	
$\hat{\psi}_s$	-0.01	MPa	
$\psi_{s,sat}$	-1.7×10^{-4} (loamy sand) -7×10^{-4} (sandy loam)	MPa	(Laio et al., 2001)

	-1.43×10^{-3} (loam)		
Energy balance parameters			
f_{cloud}	0.1 (i.e., clear sk~~iesy~~)	-	
f_{NIR}	0.55	-	(Campbell and Norman, 1998)
f_{PAR}	1-f_{NIR}	-	(Campbell and Norman, 1998)
$K_{bl,d}$	0.8	-	(Campbell and Norman, 1998)
$\varepsilon_{a,clear}$	9.2 $10^{-6}T_a^2$	-	(Swinbank equation; Campbell and Norman, 1998)
ε_c	0.97	-	(Campbell and Norman, 1998)
ρ_i	0.057 (i=PAR) 0.389 (i=NIR)	-	(Leuning et al., 1995)
σ_i	0.2 (i=PAR) 0.8 (i=NIR)	-	(Leuning et al., 1995; Goudriaan and Van Laar, 1994)
Numerical simulation parameters			
Max_{iter}	15	-	
$T_{c,toler}$	0.1	°C	
$\psi_{c,toler}$	0.001	MPa	

S2 Model behaviour

The temporal evolution of key model variables during a soil moisture dry down, assuming constant air temperature at 25 °C, is presented in Fig. S1, and the dependences on soil moisture in Fig. S2. As soil moisture decreased, the canopy-to-air temperature difference $T_c - T_a$ and the marginal water use efficiency λ_w increased; while maximum carboxylation rate $V_{c,max}$, net CO_2 assimilation rate A_{net}, total leaf-level conductance to water vapor $g_{v,l}$, and the leaf, root and soil water potentials (ψ_l, ψ_r and ψ_s) rapidly became more negative. Conversely, all the variables were largely independent of soil moisture under well-watered conditions.

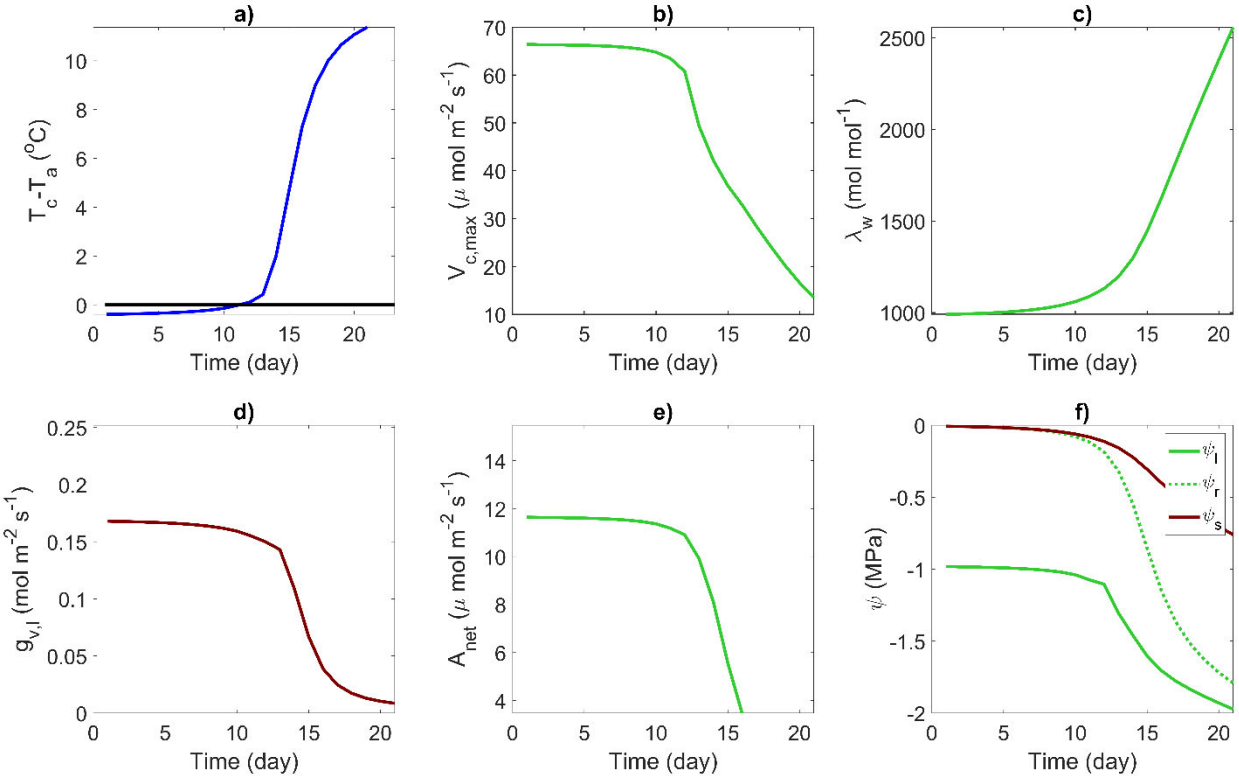

Figure S1: Temporal evolution of the key model variables during a dry down with $T_a = 25$°C: a) canopy temperature difference $T_c - T_a$, b) maximum carboxylation rate $V_{c,max}$, c) marginal water use efficiency λ_w, d) total leaf-level conductance to water vapor $g_{v,l}$, e) net CO_2 assimilation rate A_{net}, f) leaf, root, and soil water potentials, ψ_l, ψ_r and ψ_s. The black horizontal line in a) corresponds to $T_c - T_a = 0$.

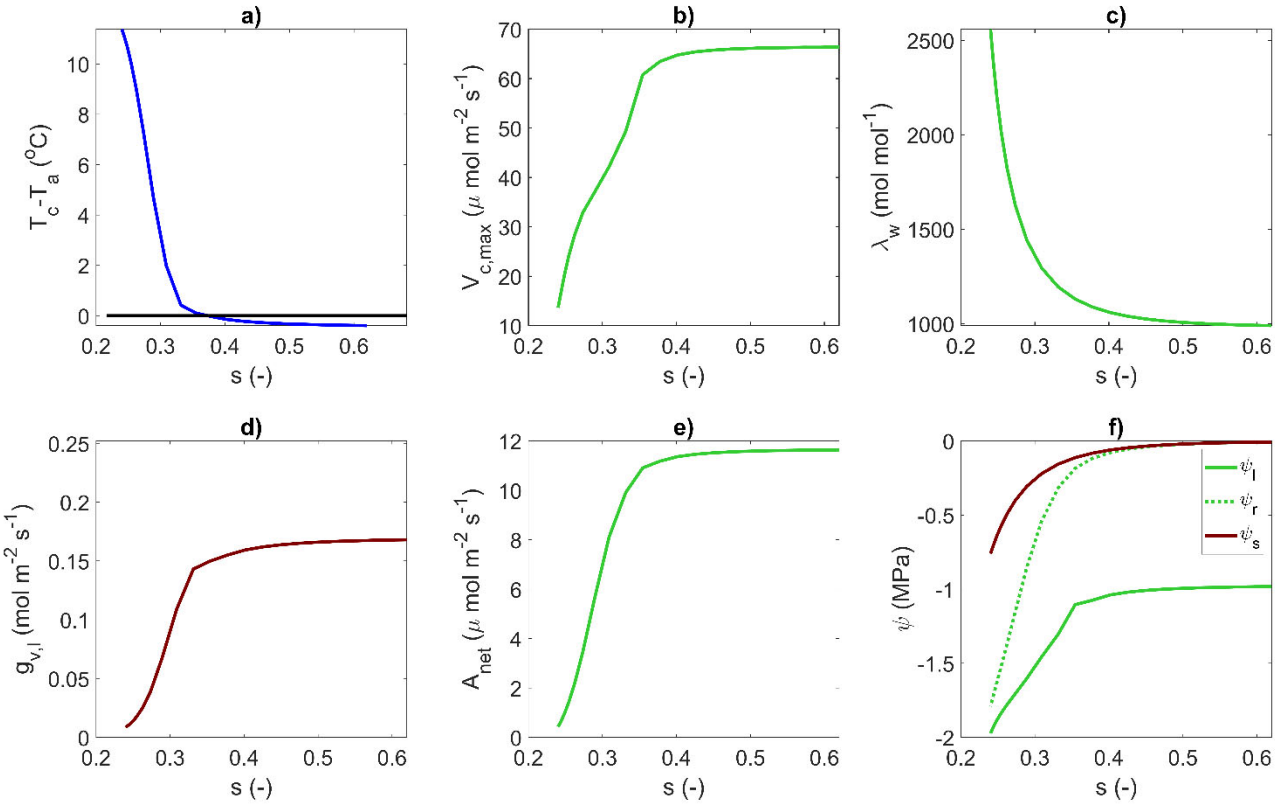

Figure S2: Dependence of the key variables on soil moisture s: a) canopy temperature difference $T_c - T_a$, b) maximum carboxylation rate $V_{c,max}$, c) marginal water use efficiency λ_w, d) total leaf-level conductance to water vapor $g_{v,l}$, e) net CO_2 assimilation rate A_{net}, f) leaf, root, and soil water potentials, ψ_l, ψ_r and ψ_s. The black horizontal line in a) corresponds to $T_c - T_a = 0$.

S3 Additional results

S3.1 Water fluxes

The dominant loss from the soil water balance occurred via evapotranspiration, with deep percolation and runoff playing a secondary role in all climatic and irrigation scenarios (Fig. S3, S4). Larger average precipitation totals (Fig. S3 far right), larger more intermittent precipitation events and irrigation applications (Fig. S4 pink and blue hues) increase the extent and variability of losses via runoff and deep percolation, although their quantitative role remains secondary when compared to cumulated evapotranspiration (compare panels in Fig. S3 and S4).

There was a large variability of the cumulated soil water fluxes relative to cumulated precipitation across the 500 simulated 21-day anthesis. The ratio of cumulated evapotranspiration and cumulated deep percolation and runoff over cumulated precipitation can exceed 1, when there was a net reduction in the soil water storage from the beginning to the end of the 21-day anthesis.

Irrigation exceeded the cumulated precipitation, in particular under larger but more intermittent precipitation (Fig. S5). This precipitation scenario also led to larger variability in cumulated irrigation inputs, in particular under higher long-term average air temperatures. Also the median number of irrigation applications per 21-day period increased from 1 at long-term air average temperature of 20 °C and for the baseline precipitation scenario at 25 °C, to 2 in the more intermittent precipitation at 25 °C and at 30 °C. Given the short duration of the period considered, it is not possible to discern smaller differences in number of irrigation applications and hence irrigation frequencies across climatic regimes.

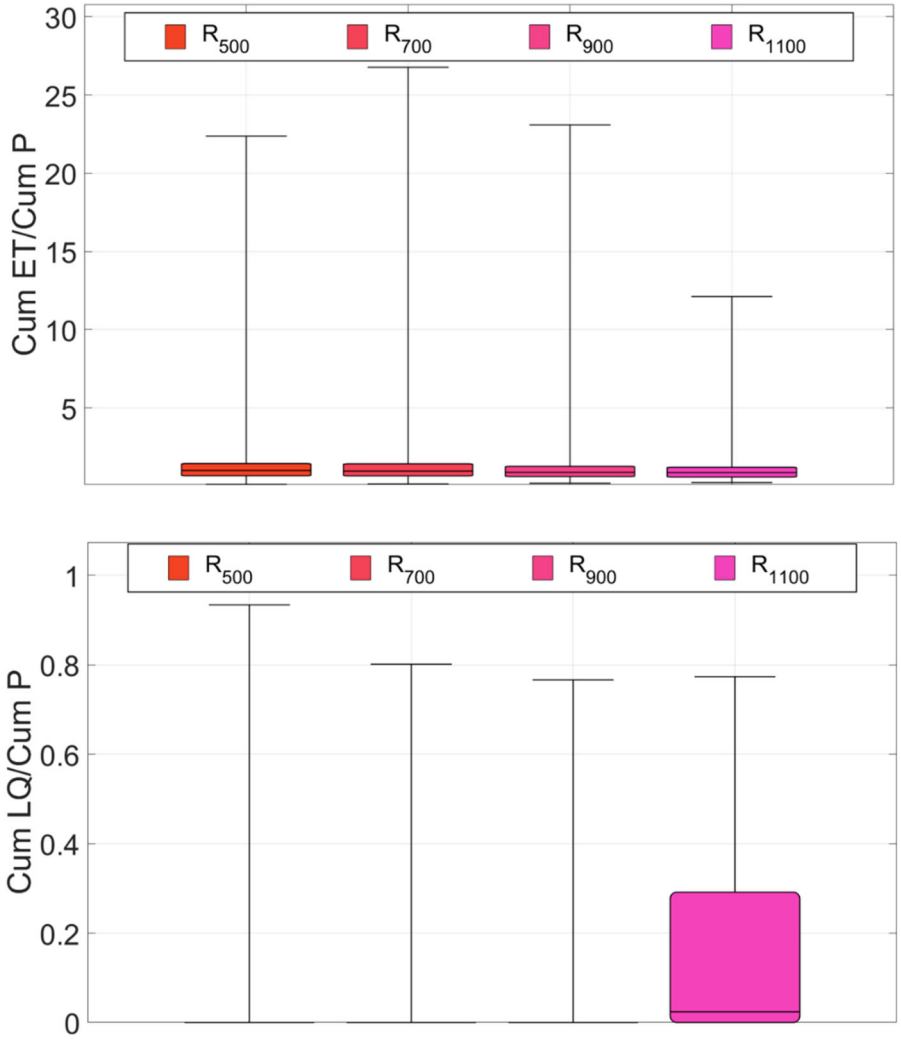

Figure S3: Distribution of the ratios of 21-day cumulated evapotranspiration (cum ET; top) and runoff and deep percolation (cum LQ; bottom) to cumulated precipitation (cum P), for four average annual precipitation totals (500, 700, 900, 1100 mm; colors), for long-term average air temperature $\mu_{T_a} = 25$ °C. The precipitation scenarios are the same as those in Fig. 4 in the main text, i.e., average precipitation depth α_p was kept at 15 mm, while average precipitation frequency λ_p changed within each group of 4 boxes from left to right, from 0.091 to 0.137, 0.183, and 0.228 d^{-1}. While in all cases 500 21-day simulations were run, ratios were not defined (and hence not included) when no precipitation was recorded over the 21-day period (from left to right, in 18, 8, 2, and 1 % of the simulations). The horizontal dark lines are the median values; the boxes extend from the first to the third quartile; whiskers cover the whole range.

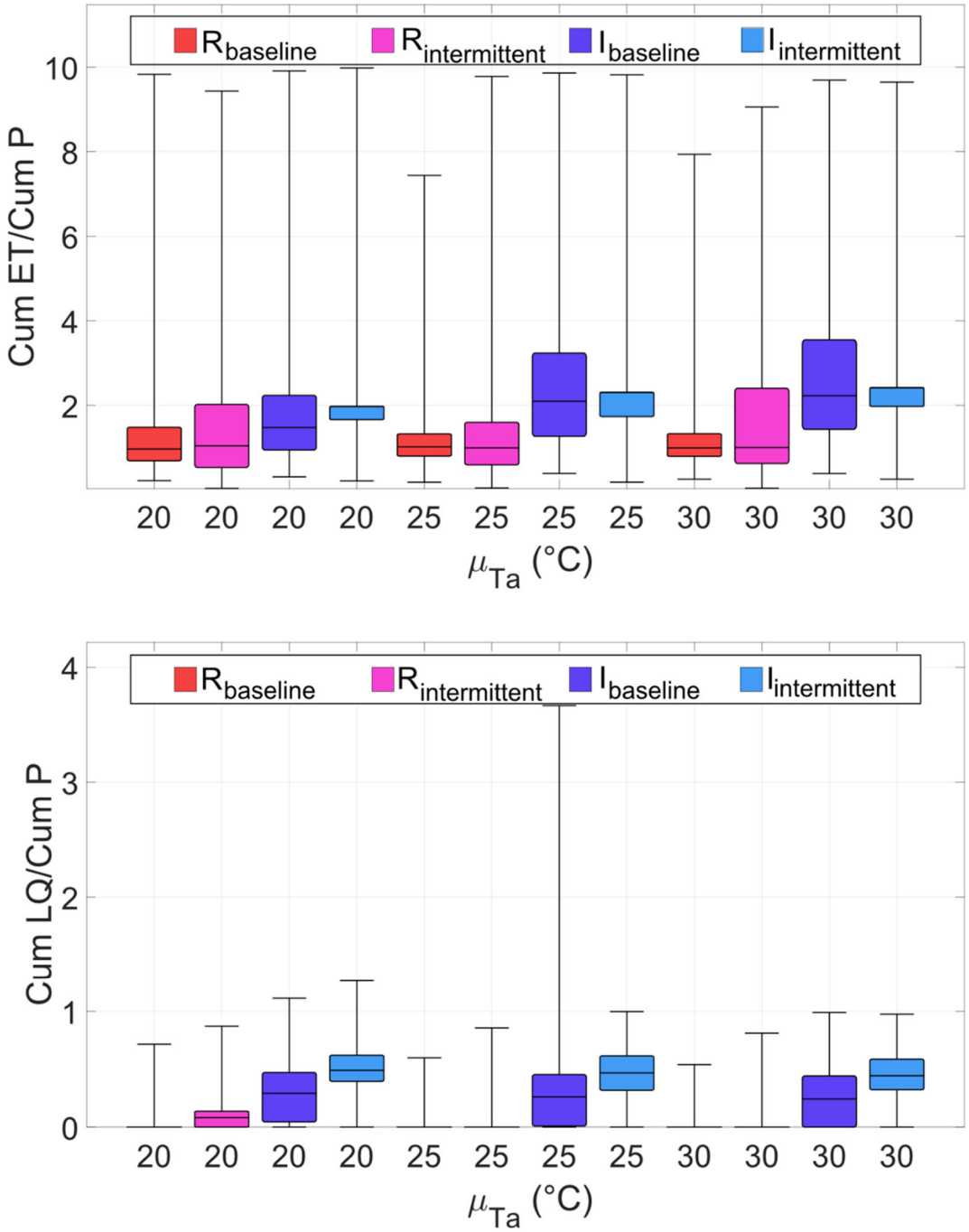

Figure S4: Distribution of the ratios of 21-day cumulated evapotranspiration (cum ET; top) and runoff and deep percolation (cum LQ; bottom) to cumulated precipitation (cum P), under three long-term average air temperatures μ_{T_a} (x-axis) and different precipitation and irrigation scenarios (colors). The climatic and irrigation scenarios are as in Fig. 5 in the main text: in each group of 4 boxes, from left to right, $R_{baseline}$ and $R_{intermittent}$ represent rainfed

cropping, respectively under baseline precipitation (α_p=8.2 mm; λ_p=0.2 d^{-1}) and more intermittent precipitation (α_p=23.5 mm; λ_p=0.07 d^{-1}); $I_{baseline}$ and $I_{intermittent}$ refer to stress avoidance irrigation, under the same precipitation regimes of the corresponding rainfed cases. While in all cases 500 21-day simulations were run, ratios were not defined (and hence not included) when no precipitation was recorded over the 21-day period (between 1 and 2 % of the simulations for the baseline precipitation scenario; and between 21 and 25 % of the simulations for the more intermittent precipitation scenario). The horizontal dark lines are the median values; the boxes extend from the first to the third quartile; whiskers cover the whole range.

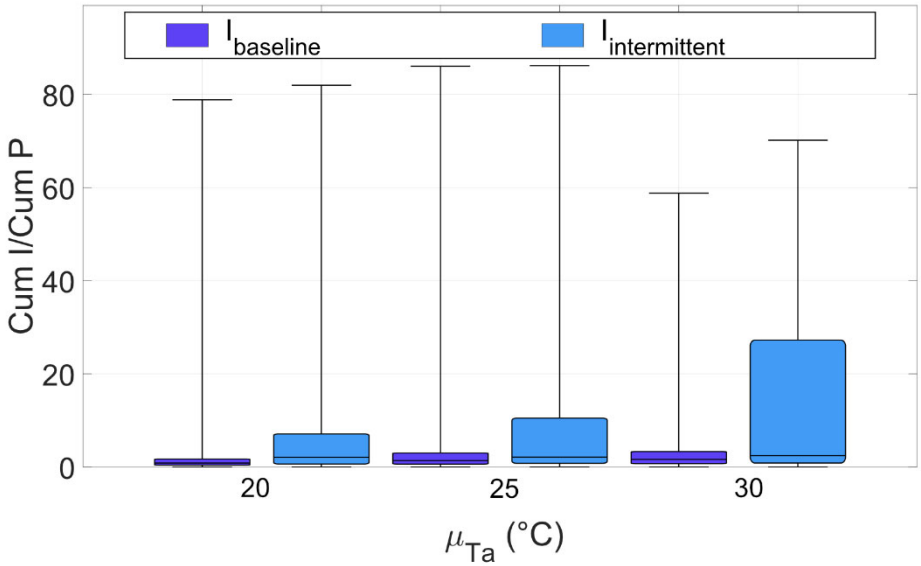

Figure S5: Distribution of the ratios of 21-day cumulated irrigation (cum I) to cumulated precipitation (cum P), under three long-term average air temperatures μ_{T_a} (x-axis) and different precipitation scenarios (colors). The climatic and irrigation scenarios are as in Fig. 5 in the main text and Fig. S5: in each pair of 2 boxes, from left to right, $I_{baseline}$ and $I_{intermittent}$ represent stress avoidance irrigation, respectively under baseline precipitation (α_p=8.2 mm; λ_p=0.2 d^{-1}) and more intermittent precipitation (α_p=23.5 mm; λ_p=0.07 d^{-1}). The number of datapoints for each box is the same as Fig. S5. The horizontal dark lines are the median values; the boxes extend from the first to the third quartile; whiskers cover the whole range.

S3.~~1~~2 Effects of air temperature variability

We tested different air temperature variability by altering the diffusion parameter (noise 'size') k_3, to which the air temperature variance is proportional (Section S1.4.3). The patterns of T_c and P_{CHS} were independent of k_3 for rainfed conditions, but their medians and variance increased with increasing k_3 ~~diffusion parameter~~ under irrigation (Fig. S~~3~~6, Table S7).

350

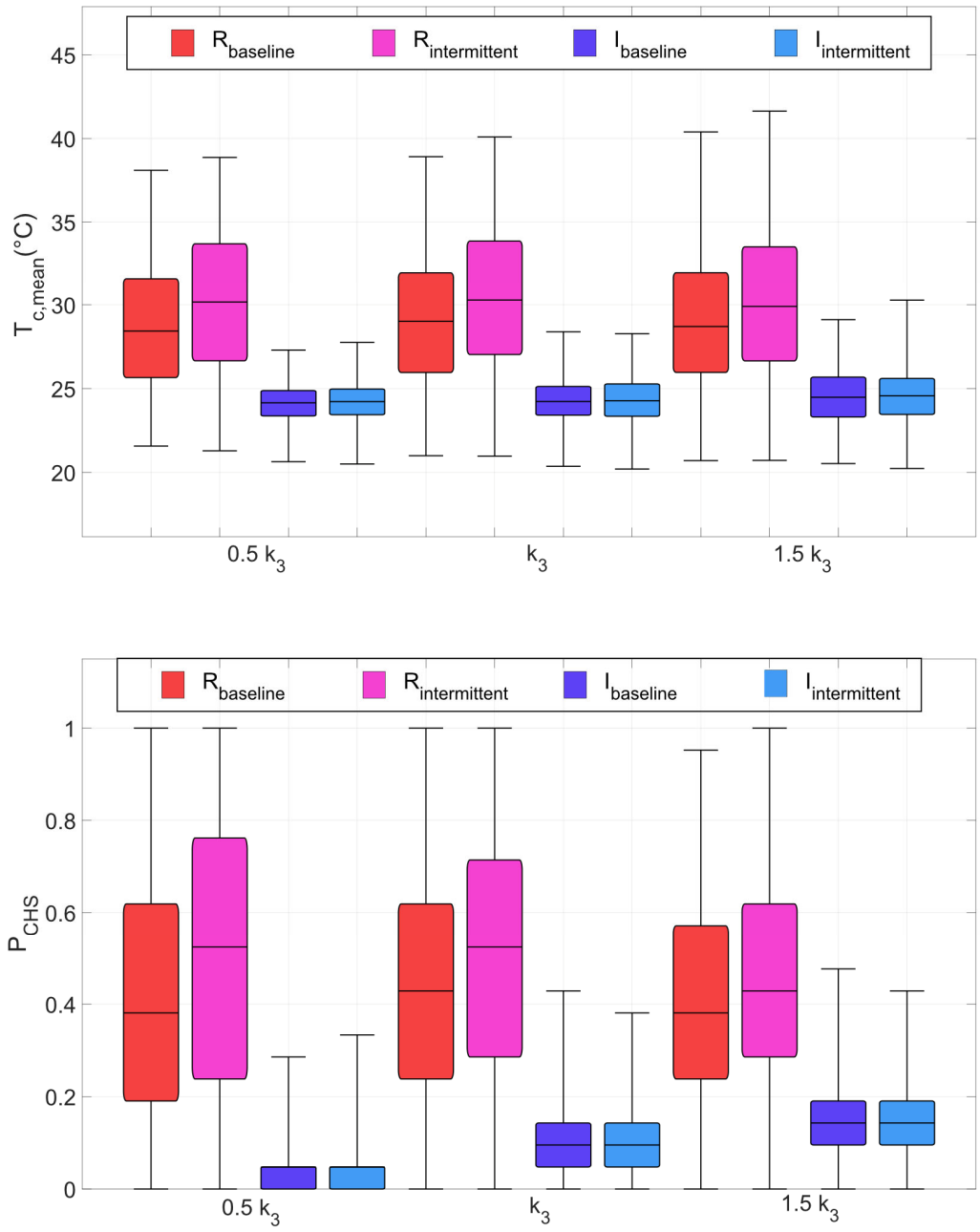

Figure S~~36:~~. Distribution of the m~~M~~ean canopy temperature during anthesis, $T_{c,mean}$ (top) and percentage of days during which $T_c > T_{th}$, P_{CHS} (bottom) under three noise 'sizes' k_3, corresponding to half of the baseline (left), baseline (center) and 1.5 times the baseline (right). Long-term ~~mean~~ average air temperature was kept at μ_{T_a}=25 °C. precipitation and irrigation scenarios are as in

Fig 5 in the main text: in each group of 4 boxes, from left to right, $R_{baseline}$ and $R_{intermittent}$ represent rainfed cropping, under baseline precipitation (α_p =8.2 mm; λ_p =0.2 d^{-1}) and more intermittent precipitation (α_p =23.5 mm ; λ_p = 0.07 d^{-1}) respectively; $I_{baseline}$ and $I_{intermittent}$ refer to stress avoidance irrigation, under the same precipitation regimes as for the corresponding rainfed case. For each climatic scenario, 500 21-day simulations were run. The horizontal dark lines are the median values; the boxes extend from the first to the third quartile; whiskers cover the whole range.

S3.23 Effects of soil texture

Soil texture determines the soil water storage capacity, the losses below the rooting zone, and the ability of the plant to take up water. Despite these potential roles of soil texture on soil and water plant dynamics, soil texture had no effect on median and variance of $T_{c,mean}$ and P_{CHS}, although the differences induced by the precipitation regime remained (Fig. S47, Table S8).

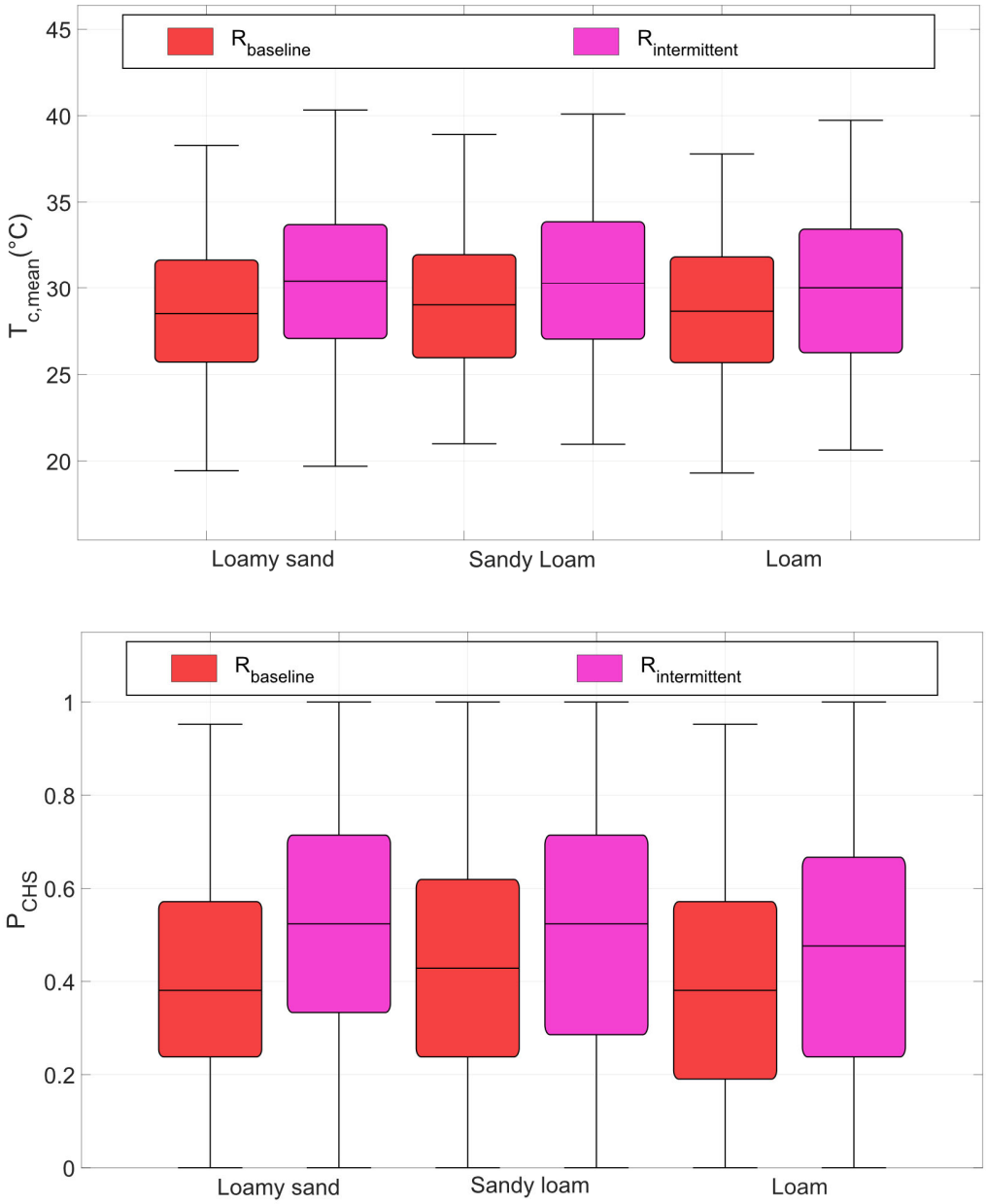

Figure S47: Distribution of mMean canopy temperature during anthesis, $T_{c,mean}$ (top) and percentage of days during which $T_c > T_{th}$, P_{CHS} (bottom) for three soil types: from left to right, loamy sand (baseline), sandy loam (baseline), and loam. $R_{baseline}$ and $R_{intermittent}$ represent rainfed cropping, under baseline precipitation (α_p =8.2 mm ; λ_p =0.2 d^{-1}) and more intermittent precipitation (α_p =23.5 mm; λ_p = 0.07 d^{-1}) respectively. For each precipitation scenario and soil type, 500 21-day simulations were run. The horizontal dark lines are the median values; the boxes extend from the first to the third quartile; whiskers cover the whole range.

S3.~~3~~4 Effects of solar radiation, wind velocity, and air relative humidity

We tested the sensitivity of T_c to radiation $Q_0^{\downarrow}$, wind velocity U, and relative humidity RH, at different soil moistures (Fig. S~~8~~5). Higher $Q_0^{\downarrow}$ led to higher T_c. Lower U enhanced canopy temperature at low soil moisture. High RH slightly increased T_c at high soil moisture.

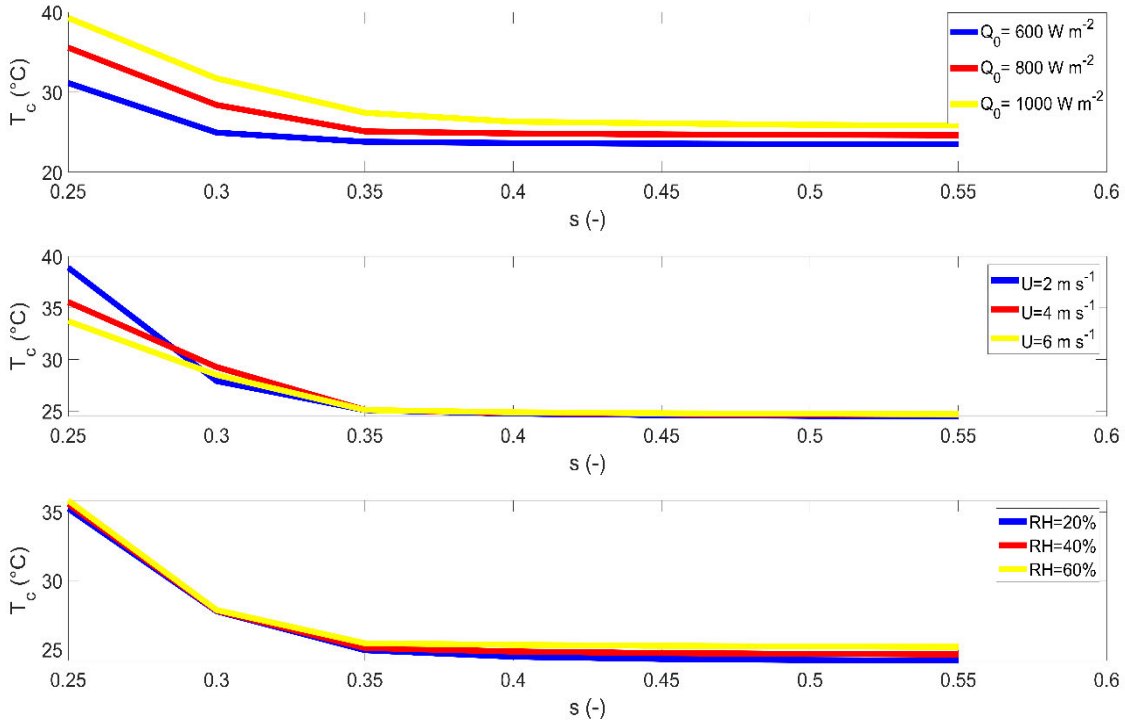

Figure S~~8~~5: Canopy temperature, T_c, as a function of soil moisture, s, as obtained for three levels of short-wave radiations $Q_0^{\downarrow}$ (top), wind velocity U (center), and relative humidity RH (bottom). All the other parameters are as in Table S2.

S4 Statistical tests

We tested whether medians and variance of $T_{c,mean}$ and P_{CHS} differed between pedoclimatic scenarios, by means of Mood~~'s~~ median test and Brown-Forsythe~~'s~~ test of equal variance. Results are summarized in Table S3 to S8.

Table S3: Statistical tests of the effects of average annual precipitation totals ~~amount~~ at different long-term ~~mean~~ average air temperature, μ_{T_a} (columns), based on 500 simulations. For each test, the test statistics (top) and p value (bottom) are reported. The degrees of freedom (df) are specified for each type of test. Data are summarized in Fig. 4 in the main text.

		20 °C	**25 °C**	**30 °C**
$T_{c,mean}$	Test on equal median df=3	232.02 <0.001	21328.78 <0.001	177.49 <0.001
	Test on equal variance df=[3, 1996]	42.36 <0.001	19.38 ~~20.82~~ <0.001	7.97 <0.001

Table S4: Statistical tests of the effects long-term ~~mean~~ average air temperatures for different average annual precipitation totals (from 500 to 1100 mm; columns), based on 500 simulations. For each test, the test statistics (top) and p value (bottom) are reported. The degrees of freedom (df) are specified for each type of test. Data are summarized in Fig. 4 in the main text.

		500 mm	**700 mm**	**900 mm**	**1100 mm**
$T_{c,mean}$	Test on equal median df=2	5682.6280 <0.001	571.7366.27 <0.001	692.3450 <0.001	785.34 ~~825.14~~ <0.001
	Test on equal variance df=[2,1497]	4.255 <0.05	12.6687 <0.001	136.70 <0.001	457.8243 <0.001

Table S5: Statistical tests of the effects of precipitation patterns and irrigation at different long-term ~~mean~~ average air temperatures, based on 500 simulations. For each test, the test statistics (top) and p value (bottom) are reported. The degrees of freedom (df) are specified for each type of test. Data are summarized in Fig. 5 in the main text.

		20 °C				**25 °C**				**30 °C**			
		Effect of precipitation pattern		Effect of irrigation		Effect of precipitation pattern		Effect of irrigation		Effect of precipitation pattern		Effect of irrigation	
		Rainfed	Irrigated	Baseline precipitation	More intermittent precipitation	Rainfed	Irrigated	Baseline precipitation	More intermittent precipitation	Rainfed	Irrigated	Baseline precipitation	More intermittent precipitation
		$R_{baseline}$ vs $R_{intermittent}$	$I_{baseline}$ vs $I_{intermittent}$	$R_{baseline}$ vs $I_{baseline}$	$R_{intermittent}$ vs $I_{intermittent}$	$R_{baseline}$ vs $R_{intermittent}$	$I_{baseline}$ vs $I_{intermittent}$	$R_{baseline}$ vs $I_{baseline}$	$R_{intermittent}$ vs $I_{intermittent}$	$R_{baseline}$ vs $R_{intermittent}$	$I_{baseline}$ vs $I_{intermittent}$	$R_{baseline}$ vs $I_{baseline}$	$R_{intermittent}$ vs $I_{intermittent}$
$T_{c,mean}$	Test on equal median df=1	~~17.42~~32.40 <0.001	0.02~~3.14~~ ~~0.08~~0.90	~~138.381~~53.66 <0.001	345.74~~2~~~~87.30~~ <0.001	12.54 <0.001	0.78~~14~~ 0.38~~7~~	360.003~~45.74~~ <0.001	484.42 <0.001	~~16.38~~26.90 <0.001	~~0.78~~0.00 ~~0.38~~1.00	467.864~~84.42~~ <0.001	602.18~~5~~~~01.26~~ <0.001
	Test on equal variance df=[1,998]	~~13.32~~18.49 <0.001	~~1.17~~0.99 0.32~~28~~	~~316.453~~23.56 <0.001	~~478.065~~00.80 <0.001	~~6.39~~4.85 <0.05	~~1.39~~0.06 0.81~~24~~	374.004~~68.75~~ <0.001	~~457.524~~83.39 <0.001	~~4.11~~9.93 <0.05	0.00~~55~~ 1.00~~0.4~~ ~~6~~	~~328.222~~46.36 <0.001	~~417.163~~27.12 <0.001
P_{CHS}	Test on equal median df=1	2~~30~~.11~~2~~~~2~~ <0.001	~~1.34~~0.1~~32~~.32 ~~20.13~~20~~.25~~	~~302.943~~54.53 <0.001	~~427.855~~12.98 <0.001	~~22.03~~13.00 <0.001	0.71 0.40	~~490.964~~78.33 <0.001	~~521.105~~58.39 <0.001	~~15.40~~8.83 <0.0~~0~~1	0.~~79~~90 0.3~~74~~	~~472.214~~99.48< 0.001	~~446.805~~63.33< 0.001
	Test on equal variance df=[1,998]	~~16.454~~1.06 <0.001	2.20~~08~~ 0.1~~45~~	~~394.095~~13.44 <0.001	~~723.337~~82.66 <0.001	~~5.55~~4.38 <0.05	0.04~~19~~ 0.84~~67~~	~~536.664~~88.02 <0.001	~~590.335~~88.32 <0.001	1.36~~0.8~~~~4~~ 0.24~~36~~	3.60~~0.0~~~~4~~ 0.8~~4~~06	89.60~~116.85~~ <0.001	~~131.578~~2.91 <0.001

Table S6: Statistical tests of the effects of long-term ~~mean~~ average air temperatures for different precipitation patterns and irrigation, based on 500 simulations. For each test, the test statistics (top) and p value (bottom) are reported. The degrees of freedom (df) are specified for each type of test. Data are summarized in Fig. 5 in the main text.

		Rainfed		**Irrigated**	
		Baseline precipitation	More intermittent precipitation	Baseline precipitation	More intermittent precipitation
$T_{c,mean}$	Test on equal median df=2	66440.6219 <0.001	534.9335 <0.001	984.2611 <0.001	980.211000 <0.001
	Test on equal variance df=[2,1497]	2.687.19 <0.0701	0.112.55 0.8908	19.2 8.18 <0.001	5.3924.02 <0.01
P_{CHS}	Test on equal median df=2	583.2171.5 4 <0.001	457.37 473.04 <0.001	9324.670 <0.001	909.45 972.86 <0.001
	Test on equal variance df=[2,1497]	36.5727.75 <0.001	19.6692 <0.001	238.00 276.15 <0.001	336.63 292.53 <0.001

Table S7: Statistical tests of the role of air temperature variance on median and variance of canopy temperatures, for different rainfall patterns and management combinations, based on 500 simulations. For each test, the test statistics (top) and p value (bottom) are reported. The degrees of freedom (df) are specified for each type of test. Data are summarized in Fig. S63.

		Rainfed		**Irrigated**	
		Baseline precipitation	More intermittent precipitation	Baseline precipitation	More intermittent precipitation
$T_{c,mean}$	Test on equal median df=2	3.381.78 0.1841	2.131.78 0.3541	12.7411.20 <0.01	7.98 8.26 <0.05
	Test on equal variance df=[2,1497]	0.0917 0.8591	0.2481 0.4579	33.1461 <0.001	23.487 <0.001
P_{CHS}	Test on equal median df=2	4.523.86 0.140	3.677.62 0.16-<0.05	327.7584 <0.001	295.7051 <0.001
	Test on equal variance df=[2,1497]	19.2231 <0.001	27.6928.83 <0.001	68.0964.26 <0.001	65.2164.82 <0.001

Table S8: Statistical tests of the role of soil texture on canopy temperature mean and variance, based on 500 simulations. For each test, the test statistics (top) and p value (bottom) are reported. The degrees of freedom (df) are specified for each type of test. Data are summarized in Fig. S47.

		Baseline precipitation	**More intermittent precipitation**
$T_{c,mean}$	Test on equal median df=2	1.342.50 0.2951	1.460.98 0.4861
	Test on equal variance df=[2,1497]	0.3320 0.782	1.100.46 0.363
P_{CHS}	Test on equal median df=2	2.1273 0.3526	1.452.42 0.4930
	Test on equal variance df=[2,1497]	0.074 0.946	1.9047 0.1523

S5 Methodological considerations

S5.1 Modeling assumptions and their implications

The model developed does not explicitly take into account the vertical dimension, i.e., the canopy was approximated by a big leaf and the soil moisture balance was represented via a bucket-filling model.

The big-leaf approximation scales up the leaf-level carbon and water fluxes, assuming that the entire canopy is subject to the same conditions and behaves in the same way. Hence, sunlit and shaded leaves cannot be distinguished. This could underestimate the effects of solar radiation and the temperature of sunlit leaves. Indeed, T_c simulated by big-leaf model was around 1 °C higher than the simulated temperatures for shaded leaves but lower than those of sunlit leaves (Dai et al., 2004). Yet, we considered solar radiation at the top of the canopy, thus effectively representing sunlit leaves~~, i.e., providing an overestimate of the temperatures to which leaves are exposed~~. Further, the big-leaf approximation cannot capture the effects

of the wind velocity profile within the canopy, leading to canopy layers nearer to the ground to be warmer than the higher ones. These are also the layers where solar radiation is lower, thus potentially balancing out the effects of the simplifications implicit in the big-leaf framework.

The bucket-filling model assumes uniform soil moisture conditions over the active rooting zone, thus potentially underestimating the soil water availability near the soil surface soon after rainfall events and deeper in the profile later in the dry down. Hydraulic redistribution and, in general, the plant's ability to take up water at different depths limit the effects of such simplification on the modeled soil moisture (Guswa et al., 2002) and hence on the model results. Neglecting lateral flows is generally adequate in most agricultural contexts, where fields are flat and horizontally homogeneous. We also assumed instantaneous (at the daily time scale) runoff and deep percolation when soil moisture reached the threshold s_1 – just above soil field capacity. Because soil hydraulic conductivity is a highly non-linear function of soil moisture (Clapp and Hornberger, 1978), the soil drains quickly above s_1. Indeed, this simplified approach leads to soil moisture dynamics similar to those obtained including runoff as saturation excess and assuming deep percolation to be proportional to the soil hydraulic conductivity (e.g., Laio et al., 2001; not shown). The small quantitative contributions of losses via runoff and deep percolation to the soil water balance (Fig. S3 and S4) lend further support to the choice of a simplified description of these processes. The advantage of considering instantaneous losses above s_1 is that the soil moisture balance can be integrated with a daily time step – in line with that of the canopy temperature model – without significant numerical errors~~(Clapp and Hornberger, 1978).~~

While the model is capable of simulating the diurnal cycle and the whole growing season, we limited the analyses to the warmest part of the day and the crop's most sensitive developmental stage, anthesis. Similarly, the model can accommodate the temporal evolution of environmental conditions beyond air temperature fluctuations and precipitation occurrence, but we set them constant and interpreted them as averages (for RH and U) and maximum (for $Q_0^{\downarrow}$) during the simulation period. We also assumed clear skies, thus potentially overestimating canopy temperatures when compared with cloudy conditions. Taken together, these assumptions lead~~d~~ to an overestimate of T_c and hence of the frequency of canopy temperature exceeding the threshold for potential damage.

S5.2 Alternative approach to estimating canopy conductance

The soil moisture – canopy conductance relation emerging from the stomatal optimization model coupled with the SPAC (Eq. S9-S18) was compared with an empirical model of canopy ~~level~~ conductance determined based on eddy covariance data. The dependence of canopy conductance to water vapor on D~~D~~ was shown to be well approximated as (Oren et al., 1999)~~:~~

$$G_s = G_{s,ref} \cdot [1 - m \cdot \ln(P_a\, D)], \tag{S30}$$

where P_a is the air pressure (in kPa); the intercept parameter $G_{S,ref}$ is the reference surface conductance rate (mmol m^{-2} s^{-1}), corresponding to the canopy conductance at D =10^{-2} mol mol^{-1}; and the slope parameter m ([ln(kPa)]$^{-1}$) represents the sensitivity of ~~surface~~ canopy conductance to D. Both $G_{S,ref}$ and m increase with soil water availability~~, as e.g. shown by a synthesis of eddy covariance data~~ (Novick et al., 2016). For crops, a linear regression of the data presented by Novick et al. (2016) yielded

$$G_{s,ref} = 552\,\theta + 259, \quad \text{(S31)}$$

$$m = 0.57\,\theta + 0.13, \quad \text{(S32)}$$

where θ is the volumetric soil water content, related to the soil moisture s as $\theta = n\,s$, with n being the soil porosity.

During a dry down, the predicted ~~surface~~ canopy conductance obtained with the empirical approach (Eq. S30-S32) and the mechanistic model used in this work (Eq. S9-S18) were similar at air temperature T_a =20 °C, but the empirical model provided a higher value of conductance at T_a =15 °C and a lower one at T_a =25 °C and 30 °C (Fig. S~~6~~9). These discrepancies underline the importance of including mechanistically all the temperature dependences, unless site- and crop-specific data are available to correctly determine the canopy conductance empirically.

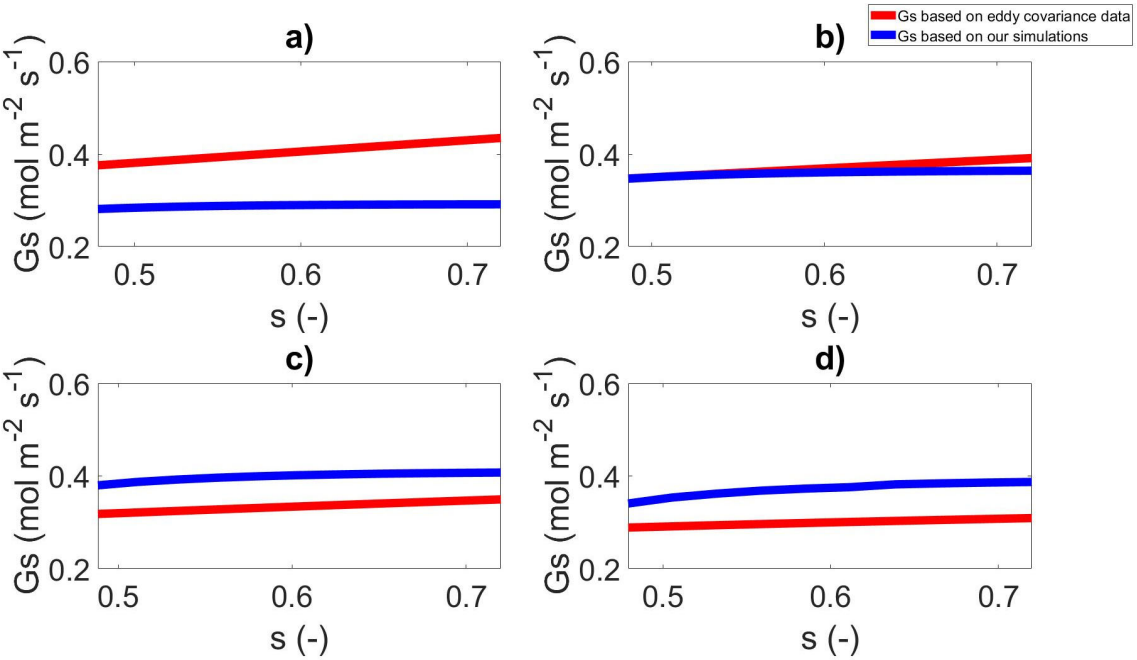

Figure S~~6~~9: ~~Comparison of two approaches to the determination of the canopy conductance for different air temperatures (a, b, c, d correspond to = 15, 20, 25, 30 °C respectively). Surface~~ Canopy conductance G_s (mol m^{-2} s^{-1}) as a function of soil moisture s, based on the upscaling of the leaf-~~-~~level optimal stomatal conductance (in blue) ~~is compared with~~and the empirical model based on eddy covariance data (Eq. S30-S32; in red) for different air temperatures (a, b, c, d correspond to T_a = 15, 20, 25, 30 °C

respectively). To avoid extrapolations, the range of soil moisture considered corresponds to that for which data on G_s are available in Novick et al. (2016).

References

Amthor, J. S.: Scaling CO_2-photosynthesis relationships from the leaf to the canopy, Photos Res, 39, 321-350, https://doi.org/10.1007/bf00014590, 1994.

Bengtson, C., Larsson, S., and Liljenberg, C.: Effects of water stress on cuticular transpiration rate and amount and composition of epicuticular wax in seedlings of six oat varieties, Physiol Plantarum, 44, 319-324, https://doi.org/10.1111/j.1399-3054.1978.tb01630.x, 1978.

Benth, F. E., and Benth, J. Š.: The volatility of temperature and pricing of weather derivatives, Quant Finance, 7, 553-561, https://doi.org/10.1080/14697680601155334, 2007.

Bernacchi, C. J., Singsaas, E. L., Pimentel, C., Portis, A. R., and Long, S. P.: Improved temperature response functions for models of Rubisco-limited photosynthesis, Plant Cell Env, 24, 253-259, https://doi.org/10.1111/j.1365-3040.2001.00668.x, 2001.

Bonan, G.: Climate change and terrestrial ecosystem modeling, Cambridge University Press, Cambridge, UK, xx+438 pp., 2019.

Campbell, G. S., and Norman, J. M.: An introduction to environmental biophysics, Springer, New York City, USA, xv+286 pp., 1998.

Clapp, R. B., and Hornberger, G. M.: Empirical equations for some soil hydraulic properties, Water Resour Res, 14, 601-604, https://doi.org/10.1093/jxb/eri174, 1978.

Dai, Y., Dickinson, R. E., and Wang, Y.-P.: A two-big-leaf model for canopy temperature, photosynthesis, and stomatal conductance, J Climate, 17, 2281-2299, https://doi.org/10.1175/1520-0442(2004)017<2281:Atmfct>2.0.Co;2, 2004.

Dingman, S.: Physical hydrology, Macmillan, New York, USA, 575 pp., 1994.

Drake, J. E., Power, S. A., Duursma, R. A., Medlyn, B. E., Aspinwall, M. J., Choat, B., Creek, D., Eamus, D., Maier, C., Pfautsch, S., Smith, R. A., Tjoelker, M. G., and Tissue, D. T.: Stomatal and non-stomatal limitations of photosynthesis for four tree species under drought: A comparison of model formulations, Agr Forest Met, 247, 454-466, https://doi.org/10.1016/j.agrformet.2017.08.026, 2017.

Duursma, R. A., Blackman, C. J., Lopéz, R., Martin-StPaul, N. K., Cochard, H., and Medlyn, B. E.: On the minimum leaf conductance: its role in models of plant water use, and ecological and environmental controls, New Phytol, 221, 693-705, https://doi.org/10.1111/nph.15395, 2019.

English, M.: Deficit Irrigation. I: Analytical Framework, Journal of Irrigation and Drainage Engineering, 116, 399-412, https://doi.org/10.1061/(ASCE)0733-9437(1990)116:3(399), 1990.

Goudriaan, J., and Van Laar, H.: Modelling potential crop growth processes. Current issues in production ecology, Kluwer Academic Publishers, Dordrecht, Netherlands, 978-994 pp., 1994.

Guswa, A. J., Celia, M. A., and Rodriguez-Iturbe, I.: Models of soil moisture dynamics in ecohydrology: A comparative study, Water Resour Res, 38, 5-1-5-15, https://doi.org/10.1029/2001wr000826, 2002.

Jackson, R. B., Canadell, J., Ehleringer, J. R., Mooney, H. A., Sala, O. E., and Schulze, E. D.: A global analysis of root distributions for terrestrial biomes, Oecologia, 108, 389-411, https://doi.org/10.1007/BF00333714, 1996.

Jarvis, P. G., and McNaughton, K. G.: Stomatal control of transpiration: Scaling up from leaf to region, in: Advances in Ecological Research, edited by: MacFadyen, A., and Ford, E. D., Academic Press, Cambridge, USA, 1-49, 1986.

Jones, H.: Plants and microclimate: a quantitative approach to environmental plant physiology, Cambridge University Press, Cambridge, UK, 428 pp., 1992.

Katul, G. G., Mahrt, L., Poggi, D., and Sanz, C.: One-and two-equation models for canopy turbulence, Bound-Lay Meteorol, 113, 81-109, https://doi.org/10.1023/B:BOUN.0000037333.48760.e5, 2004.

Katul, G. G., Palmroth, S., and Oren, R.: Leaf stomatal responses to vapour pressure deficit under current and CO_2-enriched atmosphere explained by the economics of gas exchange, Plant Cell Env, 32, 968-979, https://doi.org/10.1111/j.1365-3040.2009.01977.x, 2009.

Kerstiens, G.: Cuticular water permeability and its physiological significance, J Exp Bot, 47, 1813-1832, https://doi.org/10.1093/jxb/47.12.1813, 1996.

Laio, F., Porporato, A., Ridolfi, L., and Rodriguez-Iturbe, I.: Plants in water-controlled ecosystems: active role in hydrologic processes and response to water stress - II. Probabilistic soil moisture dynamics, Adv Water Resour, 24, 707-723, https://doi.org/10.1016/s0309-1708(01)00005-7, 2001.

Leuning, R., Kelliher, F., De Pury, D., and Schulze, E. D.: Leaf nitrogen, photosynthesis, conductance and transpiration: scaling from leaves to canopies, Plant Cell Env, 18, 1183-1200, https://doi.org/10.1111/j.1365-3040.1995.tb00628.x, 1995.

Mäkelä, A., Berninger, F., and Hari, P.: Optimal control of gas exchange during drought: Theoretical analysis, Ann Bot, 77, 461-467, https://doi.org/10.1006/anbo.1996.0056, 1996.

Mäkinen, H., Kaseva, J., Trnka, M., Balek, J., Kersebaum, K. C., Nendel, C., Gobin, A., Olesen, J. E., Bindi, M., Ferrise, R., Moriondo, M., Rodríguez, A., Ruiz-Ramos, M., Takáč, J., Bezák, P., Ventrella, D., Ruget, F., Capellades, G., and Kahiluoto, H.: Sensitivity of European wheat to extreme weather, Field Crop Res, 222, 209-217, https://doi.org/10.1016/j.fcr.2017.11.008, 2018.

Manzoni, S., Vico, G., Katul, G., Fay, P. A., Polley, W., Palmroth, S., and Porporato, A.: Optimizing stomatal conductance for maximum carbon gain under water stress: a meta-analysis across plant functional types and climates, Funct Ecol, 25, 456-467, https://doi.org/10.1111/j.1365-2435.2010.01822.x, 2011.

Manzoni, S., Vico, G., Porporato, A., and Katul, G.: Biological constraints on water transport in the soil–plant–atmosphere system, Adv Water Resour, 51, 292-304, https://doi.org/10.1016/j.advwatres.2012.03.016, 2013.

Medlyn, B., Dreyer, E., Ellsworth, D., Forstreuter, M., Harley, P., Kirschbaum, M., Le Roux, X., Montpied, P., Strassemeyer, J., and Walcroft, A.: Temperature response of parameters of a biochemically based model of photosynthesis. II. A review of experimental data, Plant Cell Env, 25, 1167-1179, https://doi.org/10.1046/j.1365-3040.2002.00891.x, 2002.

Medlyn, B. E., Duursma, R. A., Eamus, D., Ellsworth, D. S., Prentice, I. C., Barton, C. V., Crous, K. Y., De Angelis, P., Freeman, M., and Wingate, L.: Reconciling the optimal and empirical approaches to modelling stomatal conductance, Glob Change Biol, 17, 2134-2144, https://doi.org/10.1111/j.1365-2486.2010.02375.x, 2011.

Milly, P.: Climate, soil water storage, and the average annual water balance, Water Resour Res, 30, 2143-2156, https://doi.org/10.1029/94WR00586, 1994.

Novick, K. A., Ficklin, D. L., Stoy, P. C., Williams, C. A., Bohrer, G., Oishi, A. C., Papuga, S. A., Blanken, P. D., Noormets, A., Sulman, B. N., Scott, R. L., Wang, L., and Phillips, R. P.: The increasing importance of atmospheric demand for ecosystem water and carbon fluxes, Nat Clim Change, 6, 1023, https://doi.org/10.1038/nclimate3114, 2016.

Oren, R., Sperry, J. S., Katul, G. G., Pataki, D. E., Ewers, B. E., Phillips, N., and Schafer, K. V. R.: Survey and synthesis of intra- and interspecific variation in stomatal sensitivity to vapour pressure deficit, Plant Cell Env, 22, 1515-1526, https://doi.org/10.1046/j.1365-3040.1999.00513.x, 1999.

Ridolfi, L., D'Odorico, P., and Laio, F.: Noise-induced phenomena in the environmental sciences, Cambridge University Press, Cambridge, UK, 2011.

Rigby, J. R., and Porporato, A.: Spring frost risk in a changing climate, Geophys Res Lett, 35, https://doi.org/10.1029/2008gl033955, 2008.

Rodriguez-Iturbe, I., Porporato, A., Ridolfi, L., Isham, V., and Cox, D.: Probabilistic modelling of water balance at a point: the role of climate, soil and vegetation, P Roy Soc Lond A Mat, 455, 3789-3805, https://doi.org/10.1098/rspa.1999.0477, 1999.

Saini, H. S., and Aspinall, D.: Abnormal sporogenesis in wheat (*Triticum aestivum* L.) induced by short periods of high temperature, Ann Bot, 49, 835-846, https://doi.org/10.1093/oxfordjournals.aob.a086310, 1982.

Tuzet, A., Perrier, A., and Leuning, R.: A coupled model of stomatal conductance, photosynthesis and transpiration, Plant Cell Env, 26, 1097-1116, https://doi.org/10.1046/j.1365-3040.2003.01035.x, 2003.

Vico, G., and Porporato, A.: Modelling C3 and C4 photosynthesis under water-stressed conditions, Plant Soil, 313, 187-203, https://doi.org/10.1007/s11104-008-9691-4, 2008.

Vico, G., and Porporato, A.: From rainfed agriculture to stress-avoidance irrigation: I. A generalized irrigation scheme with stochastic soil moisture, Adv Water Resour, 34, 263-271, https://doi.org/10.1016/j.advwatres.2010.11.010, 2011.

Vico, G., Manzoni, S., Palmroth, S., Weih, M., and Katul, G.: A perspective on optimal leaf stomatal conductance under CO_2 and light co-limitations, Agr Forest Met, 182, 191-199, https://doi.org/10.1016/j.agrformet.2013.07.005, 2013.

Webber, H., Ewert, F., Kimball, B. A., Siebert, S., White, J. W., Wall, G. W., Ottman, M. J., Trawally, D. N. A., and Gaiser, T.: Simulating canopy temperature for modelling heat stress in cereals, Environ Modell Softw, 77, 143-155, https://doi.org/10.1016/j.envsoft.2015.12.003, 2016.

Wei, Z. W., Yoshimura, K., Wang, L. X., Miralles, D. G., Jasechko, S., and Lee, X. H.: Revisiting the contribution of transpiration to global terrestrial evapotranspiration, Geophys Res Lett, 44, 2792-2801, https://doi.org/10.1002/2016gl072235, 2017.

Wullschleger, S. D.: Biochemical limitations to carbon assimilation in C_3 plants—a retrospective analysis of the A/C_i curves from 109 species, J Exp Bot, 44, 907-920, https://doi.org/10.1093/jxb/44.5.907, 1993.

Zhou, S., Duursma, R. A., Medlyn, B. E., Kelly, J. W., and Prentice, I. C.: How should we model plant responses to drought? An analysis of stomatal and non-stomatal responses to water stress, Agr Forest Met, 182, 204-214, https://doi.org/10.1016/j.agrformet.2013.05.009, 2013.